# Synthesis and Characterization of Highly Fluorinated Tungsten(II) Metallacyclopropene Complexes. Kinetics and Mechanism of an Unprecedented $\eta^2$-Vinyl Isomerization

Jaqueline L. Kiplinger,† Thomas G. Richmond,*,† Atta M. Arif,†
Carlos Dücker-Benfer,‡ and Rudi van Eldik*,‡

*Department of Chemistry, University of Utah, Salt Lake City, Utah 84112, and Institute for Inorganic Chemistry, University of Erlangen-Nürnberg, 91058 Erlangen, Germany*

*Received December 5, 1995*⊗



This report describes a novel migratory insertion reaction which leads to the formation of highly fluorinated $\eta^2$-vinyl complexes at a tungsten(II) metal center. Insight into the nature of this transformation was obtained by isolation and crystallographic characterization of a kinetic intermediate in the insertion process. Ambient-temperature photolysis of a toluene solution of the tungsten(II) tetrafluoroaryl metallacycle **2** and perfluoro-2-butyne accesses the kinetic $\eta^2$-vinyl complex **3** in which the fluoride is *trans* to the inserted acetylene and *cis* to both carbonyl ligands. The solid-state structure of **3** has been determined. Upon heating, **3** is converted to the thermodynamic $\eta^2$-vinyl product **4** in which the fluoride ligands is now *cis* to the inserted alkyne and *trans* to one CO and *cis* to the second CO ligand. Detailed kinetic studies are reported for this isomerization reaction using both infrared spectroscopy and UV−visible spectroscopy. In the absence of added ligand, this transformation displays first-order disappearance of **3** with $\Delta H^{\ddagger} = 124(\pm 2)$ kJ/mol, $\Delta S^{\ddagger} = +48(\pm 5)$ J/(mol·K) and $\Delta V^{\ddagger} = +15.6(\pm 0.4)$ cm$^3$/mol. This is in accord with a limiting dissociative mechanism. Carbon monoxide enhances the rate of isomerization and shows first-order dependence in $p$(CO) with $\Delta H^{\ddagger} = 98(\pm 3)$ kJ/mol, $\Delta S^{\ddagger} = -5(\pm 9)$ J/(mol·K), and $\Delta V^{\ddagger} = +3.9(\pm 0.2)$ cm$^3$/mol. The P(OMe)$_3$-promoted isomerization displays saturation behavior with $\Delta H^{\ddagger} = 77(\pm 2)$ kJ/mol, $\Delta S^{\ddagger} = -46(\pm 6)$ J/(mol·K), and $\Delta V^{\ddagger} = +5.5(\pm 0.4)$ cm$^3$/mol at 2.2 M P(OMe)$_3$. The negative entropy and positive volume of activation indicate that congestion is developed in the transition state. The kinetic data for the ligand-promoted transformations are in agreement with a mechanism involving a rapid pre-equilibrium ($K$) during which the adduct species [**3**·P(OMe)$_3$] is formed, followed by a rate-determining step ($k$) to produce **5**. For this process, $k_{obs} = Kk[P(OMe)_3]/(1 + k[P(OMe)_3])$. Visible spectroscopic evidence for the adduct species [**3**·P(OMe)$_3$] has been obtained. Nonlinear least-squares analysis of the $k_{obs}$ versus [P(OMe)$_3$] plot determined a $K = 1.4 \pm 0.1$ M$^{-1}$ and a $k = (89 \pm 13) \times 10^{-5}$ s$^{-1}$, such that $kK = 1.2 \times 10^{-3}$ M$^{-1}$ s$^{-1}$ for the adduct formation. It is unlikely that an actual 20-electron species is generated since the $\eta^2$-vinyl ligand can conceivably change its hapticity and function in an $\eta^1$ mode.

## Introduction

The chemical modification and ultimate functionalization of fluorocarbons continues to provide a challenge for synthetic chemists.[1] Recently, we discovered a new method for facile transformation of strong C−F bonds into C−C bonds within the coordination sphere of a tungsten(II) metal center by sequential C−F activation and alkyne insertion (eq 1).[2] In our ongoing quest to develop metal-based reagents for the functionalization of fluorocarbons[3] we uncovered an unusual $\eta^2$-vinyl isomerization process.[2] Ambient-temperature photolysis of a toluene solution of **2** and perfluoro-2-butyne accesses the *kinetic* $\eta^2$-vinyl complex **3** in which the fluoride is *trans* to the inserted acetylene and *cis* to both carbonyl ligands. Upon heating, the *kinetic* $\eta^2$-vinyl isomer **3** is smoothly converted to the *thermodynamic* $\eta^2$-vinyl product **4** in which the fluoride ligands is now *cis* to the inserted alkyne and *trans* to one CO and *cis* to the second CO ligand (eq 2).[4] To our knowledge this

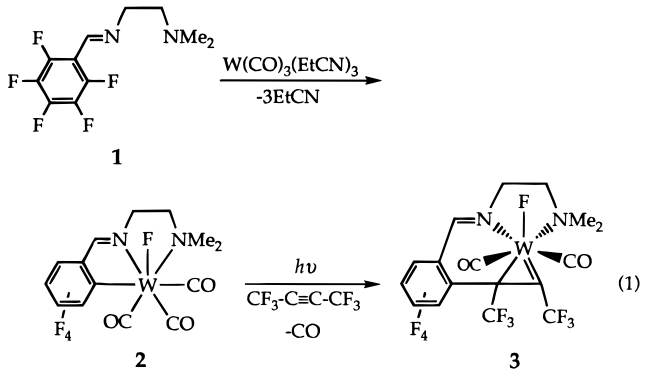


(1)

**1** **2** **3**

† University of Utah.
‡ University of Erlangen-Nürnberg.
⊗ Abstract published in *Advance ACS Abstracts,* February 15, 1996.

(1) Kiplinger, J. L.; Richmond, T. G.; Osterberg, C. E. *Chem. Rev.* **1994**, *94*, 373−431.
(2) Kiplinger, J. L.; King, M. A.; Arif, A. M.; Richmond, T. G. *Organometallics* **1993**, *12*, 3382−3384.
(3) Kiplinger, J. L.; Richmond, T. G. *J. Am. Chem. Soc.* **1996**, *118*, 1805−1806.

0276-7333/96/2315-1545$12.00/0 

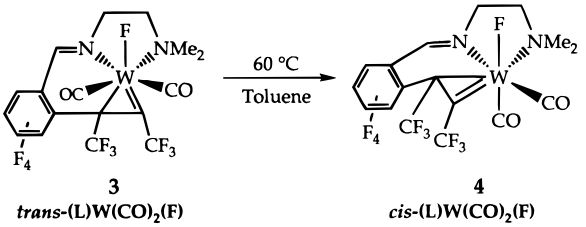


(2)

**3** ***trans*-(L)W(CO)$_2$(F)** **4** ***cis*-(L)W(CO)$_2$(F)**

system provided the first well-defined examples of alkyne insertion into a perfluoro aromatic carbon−metal bond and offered a rare opportunity to examine the kinetics of an $\eta^2$-vinyl rearrangement.

In contrast to the present work, nearly all examples of $\eta^2$-vinyl complexes are prepared by external nucleophilic attack on coordinated alkyne ligands.[5] Representative complexes prepared by Templeton (eqs 3−4),[6−8] Green (eq 5),[9,10] Reger (eq 6),[11] and Davidson (eq 7)[12] are shown in Scheme 1. If a metal is electronically

**Scheme 1**

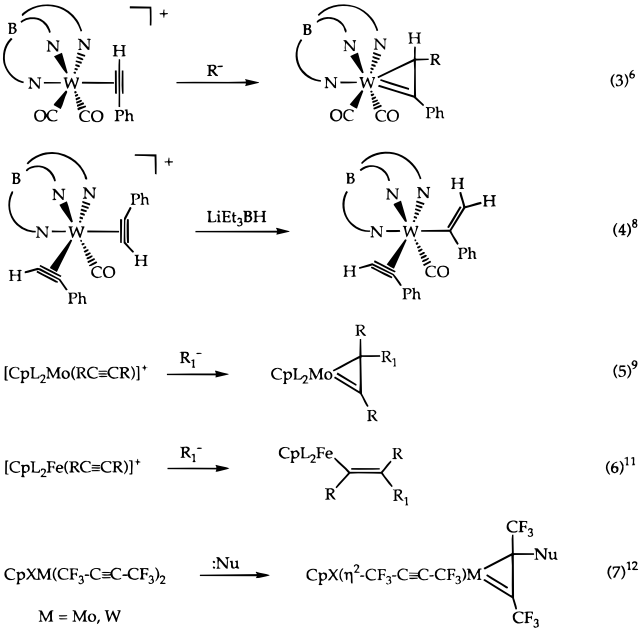


saturated, only the $\eta^1$-vinyl complex is formed.

Templeton and co-workers have elegantly demonstrated that $\eta^2$-vinyl complexes can also be formed using indirect routes. For instance, addition of an anionic dithiocarbamate ligand to the cationic butadienyl complex $[(S_2CNMe_2)_2W(\eta^4\text{-}C_4Ph_4H)]^+$ results in dechelation of the vinyl tail to form a neutral tungsten(IV) $d^2$ vinyl-substituted $\eta^2$-vinyl complex of the type $(S_2CNMe_2)_2W(\eta^2\text{-}CPh{=}CPhCPh{=}CHPh)$ (eq 8).[13] In another unusual

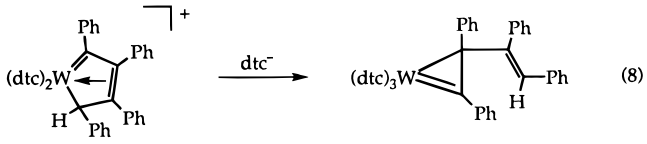


(8)

example, protonation of the carbyne complex Tp′$(CO)_2$Mo≡CN(Me)(Bu$^t$) in the presence of phenylacetylene yields the cationic $\eta^2$-vinyliminium complex [Tp′$(CO)_2$Mo($\eta^2$-C(Ph)=C(H)C(H)=N(Me)(Bu$^t$))]$^+$ which reacts with $LiEt_3BH$ to form the neutral $\eta^2$-vinylamine complex Tp′$(CO)_2$Mo($\eta^2$-C(Ph)=C(H)C(H)=N(Me)(Bu$^t$)) (eq 9).[14]

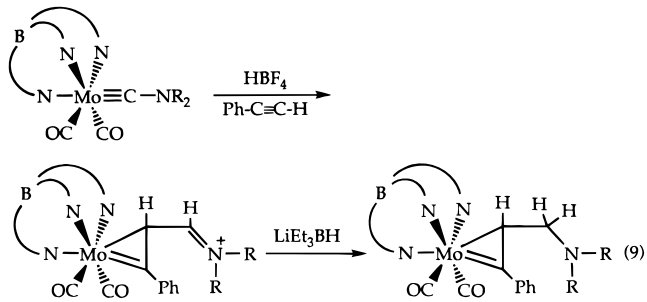


(9)

It is surprising that there have been no kinetic studies concerning $\eta^2$-vinyl processes given the postulated role of vinyl-stabilized intermediates in a variety of catalytic chemical transformations[15] and the prevalence of $\eta^2$-vinyl complexes in organometallic chemistry.[16] Although group VI $\eta^2$-vinyl systems have been the subject of a number of dynamic nuclear magnetic resonance studies (e.g. the classic windshield-wiper process),[6,9c,12c,d,14,17,18] herein we report the first detailed

(4) Throughout the remainder of the manuscript, for convenience, L will refer to the ligand chelate fragment

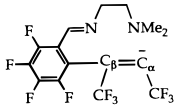

*cis* and *trans* describe the stereochemistry between the inserted alkyne ($\eta^2$-vinyl fragment) and the fluoride ligand. $F_4$-Pia refers to the ligand chelate fragment

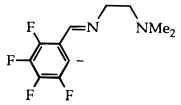

(5) For an excellent review concerning $d^4$ alkyne complexes and their related chemistry see: Templeton, J. L. *Adv. Organomet. Chem.* **1989**, *29*, 1−100.

(6) Feng, S. G.; Templeton, J. L. *Organometallics* **1992**, *11*, 2168−2175.

(7) Morrow, J. R.; Tonker, T. L.; Templeton, J. L. *J. Am. Chem. Soc.* **1985**, *107*, 6956−6963.

(8) Feng, S. G.; White, P. S.; Templeton, J. L. *J. Am. Chem. Soc.* **1992**, *114*, 2951−2960.

(9) (a) Allen, S. R.; Green, M.; Orpen, A. G.; Williams, I. D. *J. Chem. Soc., Chem. Commun.* **1982**, 826−828. (b) Green, M.; Norman, N. C.; Orpen, A. G. *J. Am. Chem. Soc.* **1981**, *103*, 1267−1269. (c) Allen, S. R.; Beevor, R. G.; Green, M.; Norman, N. C.; Orpen, A. G.; Williams, I. D. *J. Chem. Soc., Dalton Trans.* **1985**, 435−450. (d) Beevor, R. G.; Green, M.; Orpen, A.; Williams, I. D. *J. Chem. Soc., Chem. Commun.* **1983**, 673−675.

(10) Allen, S. R.; Green, M.; Norman, N. C.; Paddick, K. E.; Orpen, A. G. *J. Chem. Soc., Chem. Commun.* **1983**, 1625−1633.

(11) (a) Reger, D. L.; Belmore, K. A.; Mintz, E.; McElligot, P. J. *Organometallics* **1984**, *3*, 134−140. (b) Reger, D. L.; McElligot, P. J. *J. Am. Chem. Soc.* **1990**, *102*, 5923−5924. (c) Reger, D. L. *Acc. Chem. Res.* **1988**, *21*, 229−235.

(12) (a) Davidson, J. L.; Vasapollo, G.; Manojlović-Muir, L.; Muir, K. W. *J. Chem. Soc., Chem. Commun.* **1982**, 1025−1027. (b) Davidson, J. L.; Vasapollo, G.; Manojlović-Muir, L.; Muir, K. W. *J. Chem. Soc., Chem. Commun.* **1982**, 1025−1027. (c) Agh-Atabay, N. M.; Canoira, L. J.; Carlton, L.; Davidson, J. L. *J. Chem. Soc., Dalton Trans.* **1991**, 1175−1182. (d) Carlton, L.; Davidson, J. L. *J. Chem. Soc., Dalton Trans.* **1987**, 895−905.

(13) Feng, S. G.; Gamble, A. S.; Templeton, J. L. *Organometallics* **1989**, *8*, 2024−2031.

(14) Gamble, A. S.; White, P. S.; Templeton, J. L. *Organometallics* **1991**, *10*, 693−702.

(15) Parshall, G. W.; Ittel, S. D. *Homogeneous Catalysis*, 2nd ed.; Wiley: New York, 1992.

(16) Collman, J. P.; Hegedus, L. S.; Norton, J. R.; Finke, R. G. *Principles and Applications of Organotransition Metal Chemistry*, 2nd ed.; University Science Books: Mill Valley, CA, 1987.

(17) Carlton, L.; Davidson, J. L.; Miller, J. C.; Muir, K. W. *J. Chem. Soc., Chem. Commun.* **1984**, 11−13.

(18) Davidson, J. L.; Wilson, W. F.; Manojlović-Muir, L.; Muir, K. W. *J. Organomet. Chem.* **1983**, *254*, C6−C10.

kinetic investigation of an $\eta^2$-vinyl isomerization at a pseudo-six-coordinate tungsten(II) metal center. A portion of this work has been the subject of a preliminary communication.[2]

## Experimental Section

**General Procedures.** All manipulations involving air-sensitive reagents were performed under an atmosphere of prepurified nitrogen using standard Schlenk techniques or a Vacuum Atmosphere glovebox. Solvents were purified as follows: Tetrahydrofuran (THF) was predried with $CaH_2$ and distilled under nitrogen from sodium benzophenone ketyl radical. Diethyl ether and hexanes were predried with 4 Å molecular sieves and distilled under nitrogen from sodium benzophenone ketyl radical. Methylene chloride was predried and distilled under nitrogen from $P_2O_5$. Toluene was distilled under nitrogen from sodium metal. Trimethyl phosphite was obtained from Aldrich, distilled from sodium metal, and stored under nitrogen. Carbon monoxide and *tert*-butyl isonitrile were obtained from commercial sources and used without further purification. $^{13}CO$ was obtained from Cambridge Isotopes and used without further purification.

$^1H$, $^{13}C\{^1H\}$, $^{31}P\{^1H\}$, and $^{19}F$ NMR spectra were obtained on Varian XL-300 spectrometers at 300, 75, 121, and 281 MHz, respectively. All chemical shifts are reported in $\delta$ (ppm) units with the following abbreviations: d = doublet, m = multiplet, q = quartet, s = singlet, t = triplet, and apr = apparent. Deuterated acetone and methylene chloride $^1H$ spectra were assigned to $\delta$ 2.04 and 5.32 ppm, and $^{13}C\{^1H\}$ spectra were assigned to $\delta$ 29.8 and 53.8 ppm, respectively. For $^{19}F$ and $^{13}C\{^{19}F\}$ NMR spectra, $CFCl_3$ was used as the external reference at $\delta$ 0.00 ppm. For $^{31}P\{^1H\}$ NMR spectra 85% $H_3PO_4$ was used as the external reference at $\delta$ 0.00 ppm. Melting points were obtained in open capillary tubes and reported in °C. Mass spectra were obtained by Dr. Elliot Rachlin of the University of Utah on a Finnigan MAT 95 double-focusing high-resolution mass spectrometer operating with ionization by SIMS using a 20 keV Cesium gun. Elemental analyses were performed by Atlantic Microlab, Norcross, GA, and Desert Analytics, Tucson, AZ.

**Preparation of *trans*-{(L)W(CO)$_2$(F)} (3).** Under a nitrogen atmosphere, a 100 mL glass bomb sealed with a Teflon valve and equipped with a magnetic stir bar was cooled to −196 °C and charged with perfluoro-2-butyne (0.39 g, 2.4 mmol). In a separate Schlenk flask, a slurry of previously reported **2**[19] (0.51 g, 0.95 mmol) ($\nu_{CO}$ 2020, 1934, 1900 cm$^{-1}$) in freshly distilled toluene (30 mL) was prepared and degassed and transferred under nitrogen by syringe to the glass bomb. The resulting bright orange solution was degassed by three freeze−pump−thaw cycles and warmed to room temperature. The reaction mixture was irradiated with a Hanovia 450 W medium-pressure Hg lamp filtered through a Pyrex cell at a distance of ca. 10 cm for 160 min. Initial color change to a red-orange color was observed within 30 min, and within 160 min the solution turned a dark golden yellow color. An IR spectrum of the crude product solution confirmed the reaction was complete ($\nu_{CO}$ 2046, 1965 cm$^{-1}$). (Further irradiation leads to the generation of **4** ($\nu_{CO}$ 2020, 1915 cm$^{-1}$) as well as photochemical decomposition of **2**.) The dark golden yellow solution was evaporated to dryness, redissolved in $CH_2Cl_2$, and loaded onto a 3 in. Florisil column. A yellow band was collected with approximately 1 L of $CH_2Cl_2$. Reduction of the volume $CH_2Cl_2$ to 15 mL and addition of hexanes and cooling to −10 °C affords orange crystalline **3** in 50% yield (0.32 g, 0.47 mmol): Mp 138−140 °C; IR $\nu_{CO}$ (Nujol) 2036, 1959 cm$^{-1}$. Anal. Calcd for $WC_{17}H_{11}N_2O_2F_{11}$ (668.12 g/mol): C, 30.56; H, 1.66; N, 4.19. Found: C, 30.64; H, 1.67; N, 4.13. $^1H$ NMR ($CD_2Cl_2$) ($\delta$): N=C*H* 8.83 s, 1H; C=NC$H_2$ 5.05 m, 1H; C=NC$H_2$ 3.95 m, 1H; NC$H_2$ 3.13 m, 1H; NC$H_2$ 3.09 m, 1H; NC$H_3$ 3.04 d, 3H; NC$H_3$ 2.55 s, 3H. $^{13}C\{^1H\}$ NMR ($CD_2Cl_2$) ($\delta$): N=*C*H 158.9 s; N*C*H$_3$ 53.37 s; N*C*H$_3$ 52.48 d ($^3J_{CF}$ = 4 Hz); N*C*H$_2$ 65.61 s; N*C*H$_2$ 61.58 d ($^3J_{CF}$ = 6 Hz). $^{13}C\{^{19}F\}$ NMR ($CD_2Cl_2$) ($\delta$): CO 215.24 d ($^2J_{CF}$ = 13 Hz, $^1J_{CW}$ = 136 Hz); CO 214.97 d ($^2J_{CF}$ = 20 Hz, $^1J_{CW}$ = 184 Hz); W=$C_\alpha$CF$_3$ 196.79 dq ($^2J_{CF}$ = 40 Hz, $^2J_{CF}$ = 34 Hz); $C_\alpha$CF$_3$ 131.63 dq ($^1J_{CF}$ = 271 Hz, $^4J_{CF}$ = 29 Hz); $C_\beta$CF$_3$ 130.89 dq ($^1J_{CF}$ = 278 Hz, $^4J_{CF}$ = 37 Hz); W$C_\beta$CF$_3$ 32.4 dq ($^2J_{CF}$ = not resolved). Due to extensive C−F coupling, aryl carbon resonances could not be resolved. $^{19}F$ NMR ($CD_2Cl_2$) ($\delta$): $C_\beta$-CF$_3$ −58.32 d, 3F; $C_\alpha$CF$_3$ −59.35 d, 3F; *ortho* C−F −131.84 br, 1F; C−F −140.17 m, 1F; C−F −144.68 m, 1F; C−F −156.05 m, 1F; W−F −172.26 s, 1F.

**Preparation of *cis*-{(L)W(CO)$_2$(F)} (4).** Under a nitrogen atmosphere, a 100 mL glass bomb sealed with a Teflon valve and equipped with a magnetic stir bar was cooled to −196 °C and charged with perfluoro-2-butyne (1.38 g, 8.52 mmol). In a separate Schlenk flask, a slurry of **2** (1.00 g, 1.87 mmol) ($\nu_{CO}$ 2020, 1934, 1900 cm$^{-1}$) in freshly distilled toluene (30 mL) was prepared and degassed and transferred under nitrogen by syringe to the glass bomb. The resulting bright orange solution was degassed by three freeze−pump−thaw cycles and warmed to room temperature. The reaction mixture was heated to 80 °C for 7 h in an oil bath. Initial color change to a red-orange color was observed within 30 min, and within 7 h the solution turned a maroon color. An IR spectrum of the crude product solution confirmed the reaction was complete ($\nu_{CO}$ 2019, 1915 cm$^{-1}$). Crystallization was achieved by slowly cooling the reaction mixture to room temperature over 12 h. The solid was collected by filtration and washed with two 20 mL portions of toluene. Isolation gave 0.89 g (1.3 mmol, 67% yield) of an army-green powder **4**: Mp 138−140 °C; IR $\nu_{CO}$ (Nujol) 2026, 1925 cm$^{-1}$. Anal. Calcd for $WC_{17}H_{11}N_2O_2F_{11}\cdot{}^1/_2C_7H_8$ (714.19 g/mol): C, 34.48; H, 2.12; N, 3.92; F, 29.26. Found: C, 33.76; H, 2.02; N, 3.80; F, 28.54. Note: toluene was observed in the $^1H$ NMR spectrum. $^1H$ NMR ($CD_2Cl_2$) ($\delta$): N=C*H* 8.82 s, 1H; C=NC$H_2$ 4.77 m, 1H; C=NC$H_2$ 3.96 m, 1H; NC$H_2$ 2.91 m, 1H; NC$H_2$ 2.61 m, 1H; NC$H_3$ 3.23 s, 3H; NC$H_3$ 2.95 d, 3H. $^{13}C\{^1H\}$ NMR ($CD_2Cl_2$) ($\delta$): N=*C*H 157.2 d ($^3J_{CF}$ = 6 Hz); N*C*H$_3$ 55.9 s; N*C*H$_3$ 50.5 d ($^3J_{CF}$ = 15 Hz); N*C*H$_2$ 62.45 s; N*C*H$_2$ 61.08 d ($^3J_{CF}$ = 3 Hz). $^{13}C\{^{19}F\}$ NMR ($CD_2Cl_2$) ($\delta$): CO 221.82 d ($^2J_{CF}$ = 5 Hz, $^1J_{CW}$ = 142 Hz); CO 221.79 ($^2J_{CF}$ = 55 Hz, $^1J_{CW}$ = 150 Hz); W=$C_\alpha$CF$_3$ 202.8 dq ($^2J_{CF}$ = 41 Hz); $C_\alpha$CF$_3$ 131.2 q ($^1J_{CF}$ = 273 Hz); $C_\beta$CF$_3$ 127.9 q ($^1J_{CF}$ = 278 Hz); W$C_\beta$CF$_3$ 31.5 dq ($^2J_{CF}$ = not resolved). Due to extensive C−F coupling, aryl carbon resonances could not be resolved. $^{19}F$ NMR ($CD_2Cl_2$) ($\delta$): $C_\beta$CF$_3$ −58.88 apr t, 3F; $C_\alpha$CF$_3$ −60.80 apr d, 3F; *ortho* C−F −130.19 br, 1F; W−F −138.27 s, 1F; C−F −141.10 m, 1F; C−F −143.46 m, 1F; C−F −155.02 m, 1F.

**Preparation of *cis*-{(L)W(CO)(F)(P(OCH$_3$)$_3$)} (5).** A 100 mL Schlenk flask was charged with **3** (0.0497 g, 0.0744 mmol) ($\nu_{CO}$ 2046, 1965 cm$^{-1}$) and freshly distilled toluene (20 mL). The resulting yellow solution was thoroughly degassed, and P(OMe)$_3$ (0.040 mL, 0.34 mmol) was added via syringe. Within 5 h at ambient temperature the solution turned an intense magenta color. IR monitoring confirmed the reaction was complete in 15 h ($\nu_{CO}$ 1953 cm$^{-1}$). The reaction solution was filtered through Celite, and the black insoluble matter was discarded. The toluene solvent was then removed in vacuo to afford a gooey residue. The residue was dissolved in 20 mL of $CH_2Cl_2$, and then the solvent was removed in vacuo (sequence repeated three times) to eventually afford a crystalline magenta solid. The crude product was then recrystallized from $Et_2O$ (5 mL)/hexanes (25 mL) at −10 °C resulting in magenta microcrystalline **5** (0.0353 g, 59% yield): Mp 138−141 °C; IR $\nu_{CO}$ (Nujol) 1956, 1943 (sh) cm$^{-1}$. Anal. Calcd for **5**, $WC_{19}H_{20}F_{11}N_2O_4P\cdot{}^1/_2CH_2Cl_2$ (806.62 g/mol): C, 29.04; H, 2.62; N, 3.47. Found: C, 29.02; H, 2.54; N, 3.58. $^1H$ NMR ($CDCl_3$) ($\delta$): N=C*H* 8.82 s, 1H; C=NC$H_2$ 5.08 m, 1H; C=NC$H_2$ 3.82 m, 1H; NC$H_2$ 3.13 m, 1H; NC$H_2$ 2.93 m, 1H; NC$H_3$ 2.98 d, 3H; NC$H_3$ 2.56 s, 3H; P(OC$H_3$)$_3$ 3.34, d ($^3J_{PH}$ = 11 Hz), 9H.

(19) (a) Osterberg, C. E.; King, M. A.; Arif, A. M.; Richmond, T. G. *Angew. Chem., Int. Ed. Engl.* **1990**, *29*, 888−890. (b) Richmond, T. G. *Coord. Chem. Rev.* **1990**, *105*, 221−250.

$^{13}C\{^1H\}$ NMR (acetone-$d_6$) ($\delta$): CO 235.60 pair of d ($^2J_{CF}$ = 12 Hz, $^2J_{CP}$ = 7 Hz, $^1J_{CW}$ = 146 Hz); N=*C*H 160.17 s; N*C*H$_2$ 67.15 s; N*C*H$_2$ 62.30 d ($^3J_{CF}$ = 7 Hz); N*C*H$_3$ 53.32 s; N*C*H$_3$ 53.05 s; P(O*C*H$_3$)$_3$ 52.61 apr q; P(O*C*H$_3$)$_3$ 52.19 dd ($^2J_{CP}$ = 7 Hz, $^4J_{CF}$ = 3 Hz). $^{31}P\{^1H\}$ NMR (acetone-$d_6$) ($\delta$): 146.25 dd ($^2J_{PF}$ = 81 Hz, $^4J_{PF}$ = 8 Hz, $^1J_{PW}$ = 621 Hz). $^{19}F$ NMR (acetone-$d_6$) ($\delta$): C$_\alpha$-CF$_3$ −51.14 dd ($^4J_{PF}$ = 8 Hz, $^6J_{FF}$ = 27 Hz), 3F; C$_\beta$CF$_3$ −55.93 s, 3F; *ortho* C−F −131.35 m ($^6J_{FF}$ = 27 Hz), 1F; C−F −142.89 apr pair of d, 1F; C−F −149.70 apr t, 1F; C−F −159.04 apr t, 1F; W−F −177.49 d ($^2J_{PF}$ = 81 Hz), 1F. $^{13}C\{^{19}F\}$ NMR ($CDCl_3$) ($\delta$): W=C$_\alpha$CF$_3$ 189.45 m (due to extensive C−P and C−F coupling the C$_\alpha$ multiplets could not be resolved); C$_\alpha$*C*F$_3$ 131.46 q ($^1J_{CF}$ = 270 Hz); W*C*$_\beta$CF$_3$ 31.28 m (due to extensive C−P and C−F coupling the C$_\beta$ multiplets could not be resolved); C$_\beta$*C*F$_3$ 133.20 q ($^1J_{CF}$ = 277 Hz) (due to extensive C−F coupling phenyl carbon resonances could not be resolved); P(O*C*H$_3$)$_3$ 52.61 qm ($^1J_{CH}$ = 139 Hz, due to extensive C−P and C−F couplings the methyl carbon multiplets could not be resolved); P(O*C*H$_3$)$_3$ 52.19 qdd ($^1J_{CH}$ = 146 Hz, $^2J_{CP}$ = 7 Hz, $^4J_{CF}$ = 3 Hz).

**Preparation of (F$_4$-Pia)W(F)($^{13}$CO)$_3$ (6).** A 100 mL glass bomb sealed with a Teflon valve was charged with (F$_4$-Pia)W(F)(CO)$_3$ (**2**) (1.51 g, 2.82 mmol) and 30 mL of freshly distilled THF. The resulting orange slurry was degassed, placed under reduced pressure, and cooled to −196 °C. $^{13}$CO (1.12 mmol) was condensed into the reaction vessel. The mixture was then heated in an oil bath at 70 °C for 22 h. An IR spectrum revealed that the $^{13}$CO enrichment was not complete. The now dark orange solution was charged with $^{13}$CO (0.93 mmol) and heated in an oil bath at 70 °C. IR monitoring confirmed that the $^{13}$CO-substituted reaction was complete in 18 h ($\nu_{CO}$ 2019, 2011, 1999, 1989, 1973, 1932, 1925, 1904, 1868, 1831 cm$^{-1}$). The THF solvent was then removed in vacuo, and the resulting orange solid was collected by filtration, washed twice with 15 mL hexanes, and dried in vacuo to afford **6** in essentially quantitative yield. Mass spectrometry determined an approximate 30% isotopic enrichment of **6**. $^{13}C\{^1H\}$ NMR ($CDCl_3$) ($\delta$): CO 232.55 ($^2J_{CF}$ = 41 Hz, $^1J_{CW}$ = 116 Hz); CO 221.58 ($^2J_{CF}$ = 14 Hz, $^1J_{CW}$ = 132 Hz); CO 218.76 ($^2J_{CF}$ = 6 Hz, $^1J_{CW}$ = 122 Hz).

**Crystallography. X-ray Structure of *trans*-{(L)W(CO)$_2$(F)} (3).** An orange prism was obtained by layering a $CH_2Cl_2$ solution of **3** with hexanes and cooling to −10 °C. Data were collected at ambient temperature on an Enraf-Nonius CAD-4 diffractometer with Mo Kα radiation, using the $\omega-2\theta$ scan technique (4.00° < 2$\theta$ < 50.00°) for a crystal of dimensions 0.42 mm × 0.39 mm × 0.19 mm, mounted on a glass fiber.

Cell constants were obtained from 25 reflections with 10° < 2$\theta$ < 25°. The space group (P*bca*, No. 61) was determined from systematic absences (0*kl*, $k = 2n + 1$; *n*0*l*, $l = 2n + 1$; *hk*0, $h = 2n + 1$) and subsequent least-squares refinement. Standard reflections showed no decay during data collection. Lorentz, polarization, and empirical absorption ($\psi$ scans) corrections were applied. The structure was solved by the standard heavy-atom techniques with SPD/VAX package.[20]

Of 2410 reflections collected at ambient temperature, 2409 of these had $I > 3\sigma(I)$ and were used in the solution and refinement (SDP PLUS software). Final refinement included all non-hydrogen atoms as anisotropic contributions and hydrogens as fixed isotropic contributions. The hydrogen atoms on C10, C11, and C12 were located but were not refined. Scattering factors, and $\Delta f'$ and $\Delta f''$ values, were taken from the literature.[21] For 299 parameters, $R = 0.0378$, $R_w = 0.0411$, and the highest peak in the final map was 1.499 e/Å$^3$ (about 1.05 Å from the W atom).

**X-ray Structure of *cis*-{(L)W(CO)$_2$(F)} (4).** A dark red prism was obtained by slow crystallization from a toluene solution of **4** at room temperature. Data were collected at ambient temperature on an Enraf-Nonius CAD-4 diffractometer with Mo Kα radiation, using the $\omega-2\theta$ scan technique (4.00° < 2$\theta$ < 50.00°) for a crystal of dimensions 0.32 mm × 0.25 mm × 0.15 mm, mounted on a glass fiber.

Cell constants were obtained from 25 reflections with 10° < 2$\theta$ < 25°. The space group ($P\bar{1}$, No. 2) was determined from least-squares refinement. Standard reflections showed no decay during data collection. Lorentz, polarization, and empirical absorption ($\psi$ scans) corrections were applied.

Of 4384 reflections collected at ambient temperature, 4068 were unique; 3700 of these had $I > 3\sigma(I)$ and were used in the solution and refinement as detailed above. Final refinement included all non-hydrogen atoms as anisotropic contributions and hydrogens as fixed isotropic contributions. All the hydrogen atoms were located and their positions refined. For 385 parameters, $R = 0.0207$, $R_w = 0.0266$, and the highest peak in the final map was 0.477 e/Å$^3$.

**Spectral Studies.** Infrared spectra were recorded in 1.0 mm or 0.1 mm $CaF_2$ cells on a BioRad Model FTS-40 FTIR spectrometer operating with a resolution of 2.0 cm$^{-1}$. Visible spectra were recorded on a Hewlett Packard Model 8452A diode array spectrophotometer in a 1.00 cm Pyrex glass cell modified for work with air-sensitive compounds and gases. Variable-temperature kinetic runs were performed employing a thermostated cell holder using a VWR Scientific Model 1166 thermostated bath (P(OMe)$_3$ studies) and a VWR Scientific Model 1110 thermostated bath (isomerization and CO studies) for temperature regulation. The temperature of the thermostated baths and the temperature of the solutions in the Pyrex cell were verified using an electronic thermocouple.

**Kinetic Methods.** All isomerization reactions were carried out under either first-order (spontaneous) or pseudo-first-order (CO- or P(OMe)$_3$-promoted) conditions with the concentration of the nucleophile at least 1 order of magnitude greater than that of the kinetic isomer **3**. Isomerization was monitored by FTIR and visible spectroscopy, and excellent agreement was obtained between the two methods.

In the FTIR studies, the spontaneous and CO-promoted reactions were initiated by immersing a Schlenk flask (equipped with a septum-covered valve) charged with a toluene solution of **3** (or **3** and added CO) into a thermostated circulating water bath. Aliquots of the reaction mixture were obtained using a gastight syringe and immediately cooled to 0 °C to quench the reaction. FTIR spectra were then obtained using a 1.0-mm $CaF_2$ septum-fitted solution IR cell. The change in absorbance at an appropriate wavelength (2100−1900 cm$^{-1}$) was recorded as a function of time. The change in absorbance (disappearance) of highest energy band of **3** (2046 cm$^{-1}$) was monitored since the low-energy band (1965 cm$^{-1}$) was obscured due to solvent subtraction problems incurred using the 1.0-mm solution IR cell. However, good agreement was also obtained when the change in absorbance (appearance) of highest energy band of **4** (2019 cm$^{-1}$) was monitored. An isosbestic point was maintained at 2037 cm$^{-1}$ throughout the course of the transformation. The room-temperature P(OMe)$_3$-promoted isomerization reactions were initiated by injecting a septum-fitted Schlenk flask containing a toluene solution of **3** with P(OMe)$_3$ using a gastight syringe. Aliquots of the reaction mixture were obtained using a gastight syringe, and then FTIR spectra were obtained using a 1.0-mm $CaF_2$ septum-fitted solution IR cell. Again, the change in absorbance (disappearance) of highest energy band of **3** was monitored.

In the UV−vis studies, the spontaneous, CO- and P(OMe)$_3$-promoted reactions were initiated by immersing a 1.0-cm glass cell charged with a toluene solution of **3** (or **3** and added CO or P(OMe)$_3$) into a thermostated (±0.5 °C) cell compartment of the spectrometer. (The components within the cell were

(20) Frenz, B. A. The Enraf-Nonius CAD 4 SPD-A Real-Time System for Concurrent X-ray Data Collection and Crystal Structure Determination. In *Computing and Crystallography*; Schenk, H., Olthof-Hazelkamp, R., van Konigveld, H., Bassi, G. C., Eds.; Delft University Press: Delft, Holland, 1978; pp 64−71.

(21) Comer, D. T.; Waber, J. T. In *International Tables for X-ray Crystallography*; Ibers, J. A., Hamilton, W. C., Eds.; Kynoch: Birmingham, England, 1974; Vol. IV, Tables 2.2B and 2.3.1, pp 72−98, 149−150.

thoroughly mixed by shaking.) The temperature of the cell was allowed to equilibrate for 5 min before spectra were obtained. The change in absorbance at an appropriate wavelength (580 nm for spontaneous and CO-promoted; 500 nm for $P(OMe)_3$-promoted) was recorded as a function of time. Isosbestic points were observed at 345, 415, and 492 nm for the spontaneous and CO-promoted reactions and at 360 and 452 nm for the $P(OMe)_3$ reaction.

Plots of $\ln(A_t)$ and $\ln(A_\infty - A_t)$ vs time were linear for more than 3 half-lives, and $k_{obsd}$ was determined from the slope of this line by least-squares analysis. Rate constants were reproducible within ±5% in independent runs.

**Volume of Activation Measurements.** All measurements were made with freshly prepared solutions in which the complex **3** concentration was $2 \times 10^{-4}$ M. The temperature was set to 60.1 °C for both the CO-independent and CO-dependent isomerization reactions. The CO-independent and CO-dependent isomerization reactions were followed spectrophotometrically at $\lambda = 580$ nm by a modified (double beam) Zeiss PMQ II and a Cary 1.3 UV−vis spectrophotometer equipped with a homemade, thermostated (±0.1 °C) high-pressure cell. The $k_1$ value was measured in CO-free toluene, and the $k_2$ value was measured in CO-saturated toluene. For the $P(OMe)_3$-promoted isomerization reactions, the temperature was set to 25 °C, and the reactions were followed spectrophotometrically at $\lambda = 500$ nm. The CO was of pa quality (Messer-Griesheim), and the $P(OMe)_3$ (Fluka) was distilled prior to use.

## Results

**Synthesis and Characterization of *trans*-{(L)W(CO)$_2$(F)} (3) and *cis*-{(L)W(CO)$_2$(F)} (4).** As depicted in eq 1, ambient-temperature visible-light photolysis of a toluene solution of **2** ($\nu_{CO}$ 2020, 1934, 1900 $cm^{-1}$) in the presence of perfluorobutyne generates a dark yellow solution with **3** as the major species ($\nu_{CO}$ 2046, 1965 $cm^{-1}$). Orange crystalline **3** is isolated in 50% yield following chromatography. Due to the extensive carbon−fluorine coupling in the $^{13}C\{^1H\}$ spectrum (Figure 1a), the identification of **3** as an $\eta^2$-vinyl or metallacyclopropenyl complex was ascertained by a series of $^{13}C\{^{19}F\}$ NMR experiments (Figure 1b−d). Broad-band $^{13}C\{^{19}F\}$ decoupling was not possible due to the large frequency range (approximately 200 ppm) in the $^{19}F$ region for **3**. Thus, several single-frequency $^{13}C\{^{19}F\}$ decoupling experiments were performed.

In the $^{13}C\{^1H\}$ spectrum (Figure 1a), $C_\alpha$ appears as a doublet of quartets at $\delta$ 196.8 ppm with $^2J_{CF} = 40$ Hz from the $CF_3$ group and $^2J_{CF} = 34$ Hz from the fluoride; the CO resonances appear as a pair of doublets at $\delta$ 214.9 ppm ($^2J_{CF} = 20$ Hz) and $\delta$ 215.2 ppm ($^2J_{CF} = 13$ Hz). The $C_\beta$ resonance was not visible in the $^{13}C\{^1H\}$ spectrum. As illustrated in Figure 1, $^{13}C\{^{19}F\}$ NMR spectra were obtained while irradiating at specific $^{19}F$ NMR resonances corresponding to the $CF_3(C_\beta)$ ($\delta$ −58.3 ppm), $CF_3(C_\alpha)$ ($\delta$ −59.4 ppm), and W−F ($\delta$ −172.26 ppm) moieties. Irradiation at the $CF_3(C_\alpha)$ $^{19}F$ resonance (Figure 1b) results in the collapse of doublet of quartets to a doublet with $^2J_{CF} = 34$ Hz indicating coupling of the $CF_3$ group to $C_\alpha$. Due to the proximity of the $CF_3(C_\beta)$ and $CF_3(C_\alpha)$ $^{19}F$ NMR resonances, appearance of a singlet at $\delta$ 32.4 ppm corresponding to $C_\beta$ was also observed. Likewise, irradiation at the W−F $^{19}F$ NMR resonance (Figure 1c) results in the collapse of doublet of quartets to a quartet with $^2J_{CF} = 40$ Hz indicating coupling of the W−F to $C_\alpha$ and providing strong spectroscopic evidence for a *trans* orientation of the inserted alkyne to the fluoride. Irradiation at the W−F resonance also results in the collapse of the pair of doublets to a pair of singlets for the carbonyl ligands demonstrating coupling to W−F. Irradiation at the $CF_3(C_\beta)$ $^{19}F$ NMR resonance (Figure 1d) results in the appearance of a singlet at $\delta$ 32.4 ppm indicating coupling of the $CF_3$ to $C_\beta$. Again, a partial collapse of the $C_\alpha$ doublet of quartets at $\delta$ 196.8 ppm to a doublet with $^2J_{CF} = 40$ Hz was observed due to the proximity of the $CF_3(C_\alpha)$ and $CF_3(C_\beta)$ $^{19}F$ NMR resonances.

The carbenoid character of $C_\alpha$ is reflected by the large downfield chemical shift,[22] whereas the four-coordinate carbon, $C_\beta$, has a significant upfield chemical shift.[23] Importantly, for **3** the fluoride was determined to be *cis* to both CO ligands ($\delta$ 214.9 ppm, $^2J_{CF} = 20$ Hz, and $\delta$ 215.2 ppm, $^2J_{CF} = 12$ Hz), leaving the inserted acetylene *trans* to the fluoride. The structure of **3** was verified crystallographically (Figure 2a).

The $^1H$ NMR for **3** displays four different highly coupled multiplet resonances ($\delta$ 5.05, 3.95, 3.13, and 3.09 ppm) for the methylene protons on the ethylene backbone; each intergrate to one proton. This nonequivalence illustrates not only the chirality of the seven-coordinate tungsten(II) metal center but also the retained coordination of the ligand in solution. Each *N*-methyl group integrates to three protons; one appears as a doublet at $\delta$ 3.04 ppm ($^4J_{HF} = 4.62$ Hz) and the other as a singlet at $\delta$ 2.55 ppm. The imine proton is a singlet at 8.83 ppm.

The $^{19}F$ NMR spectrum for **3** shows seven resonances as expected with appropriate integrations. The trifluoromethyl groups are displayed as apparent doublets ($\delta$ −58.32 and −59.35 ppm). The fluoride *ortho* to the $\eta^2$-vinyl moiety is easily recognized and appears as a distinctive broad resonance at $\delta$ −131.84 ppm. The remaining aromatic fluorides are not exceptional and are observed as highly coupled multiplet resonances at $\delta$ −140.17, −144.68, and −156.05 ppm. The W−F resonance is located farthest upfield as a singlet at $\delta$ −172.26 ppm.

The kinetic $\eta^2$-vinyl complex **3** is smoothly converted to the thermodynamic $\eta^2$-vinyl product **4** at 60 °C, indicating that **3** is indeed an intermediate in the formation of **4** (eq 2). The transformation is accompanied by a marked shift (~50 $cm^{-1}$) to lower energy in the CO stretching frequencies. Alternatively, **4** is more conveniently synthesized in a direct manner by treatment of **2** with perfluoro-2-butyne in toluene at 80 °C to give a maroon solution of **4** ($\nu_{CO}$ 2019, 1915 $cm^{-1}$), which crystallizes as an air-stable green solid product in 68% isolated yield. As with compound **3**, the $^{13}C\{^1H\}$ NMR spectrum for **4** was complex due to extensive carbon−fluorine coupling and $^{13}C\{^{19}F\}$ identical to those detailed above were performed. It was determined that complex **4** possesses the requisite $\eta^2$-vinyl $^{13}C\{^{19}F\}$ NMR chemical shifts at $\delta$ 202.8 and 40.8 ppm coinciding with $C_\alpha$ and $C_\beta$, respectively. In the $^{13}C\{^1H\}$ NMR spectrum, $C_\alpha$ appears as a quartet with $^2J_{CF} = 40.8$ Hz from the $CF_3$ group with no discernible coupling from the W−F in accord with a *cis* arrangement of the W−F and the inserted alkyne. Notable is the increased $^2J_{CF}$ coupling

(22) Nugent, W. A.; Mayer, J. M. *Metal-Ligand Multiple Bonds*; Wiley: New York, 1988.
(23) Mann, B. E.; Taylor, B. F. *$^{13}C$ NMR Data for Organometallic Compounds*; Academic Press: New York, 1981.

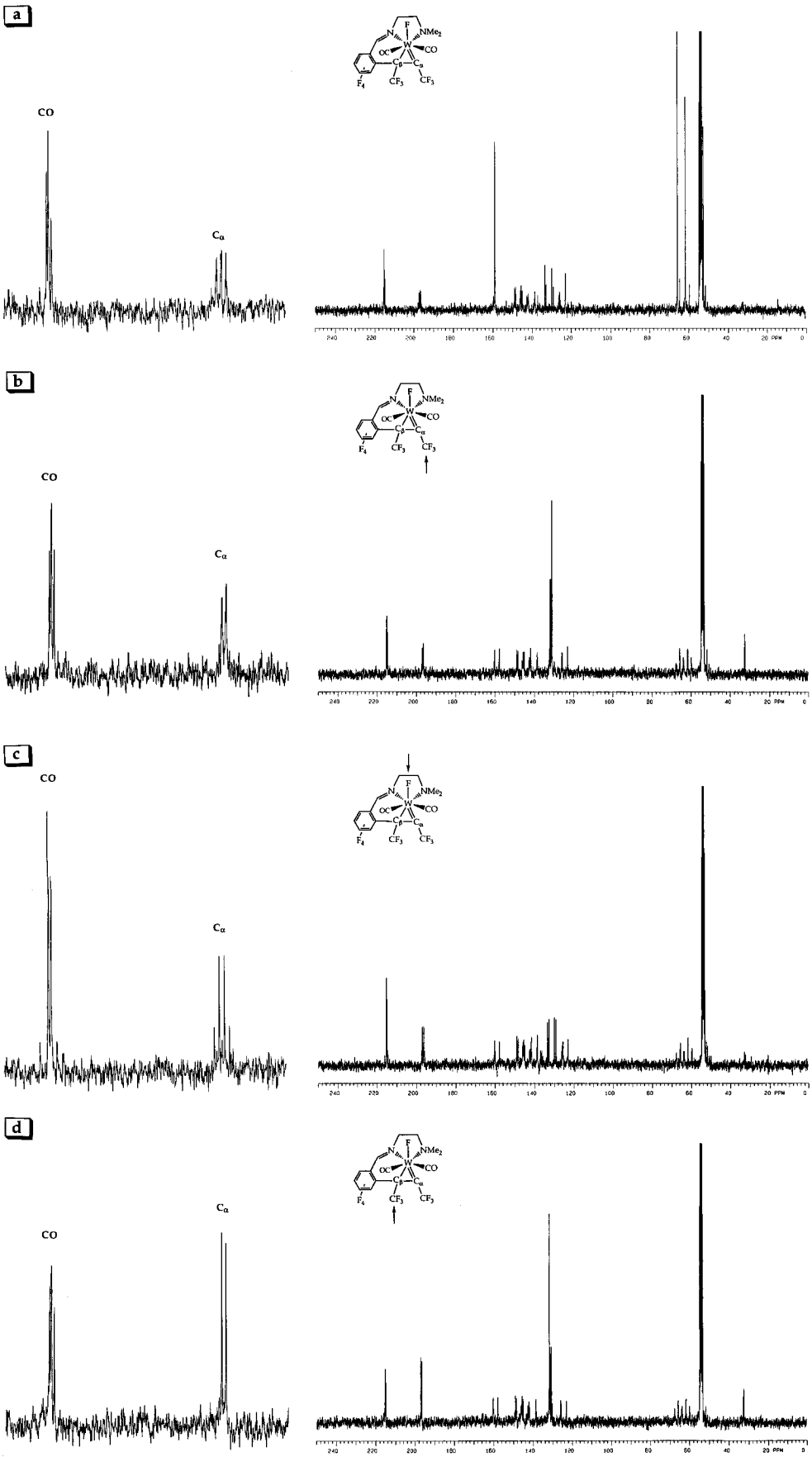


**Figure 1.** (a) $^{13}C\{^{1}H\}$ spectrum of **3**. (b) $^{13}C\{^{19}F\}$ spectrum of **3** from irradiation of the $CF_3(C_\alpha)$ resonance at $\delta$ −59.4 ppm. (c) $^{13}C\{^{19}F\}$ spectrum of **3** from irradiation of the W−F resonance at $\delta$ −172.26 ppm. (d) $^{13}C\{^{19}F\}$ spectrum of **3** from irradiation of the $CF_3(C_\beta)$ resonance at $\delta$ −58.3 ppm. The arrows indicate the fluorines irradiated in the $^{13}C\{^{19}F\}$ experiments.

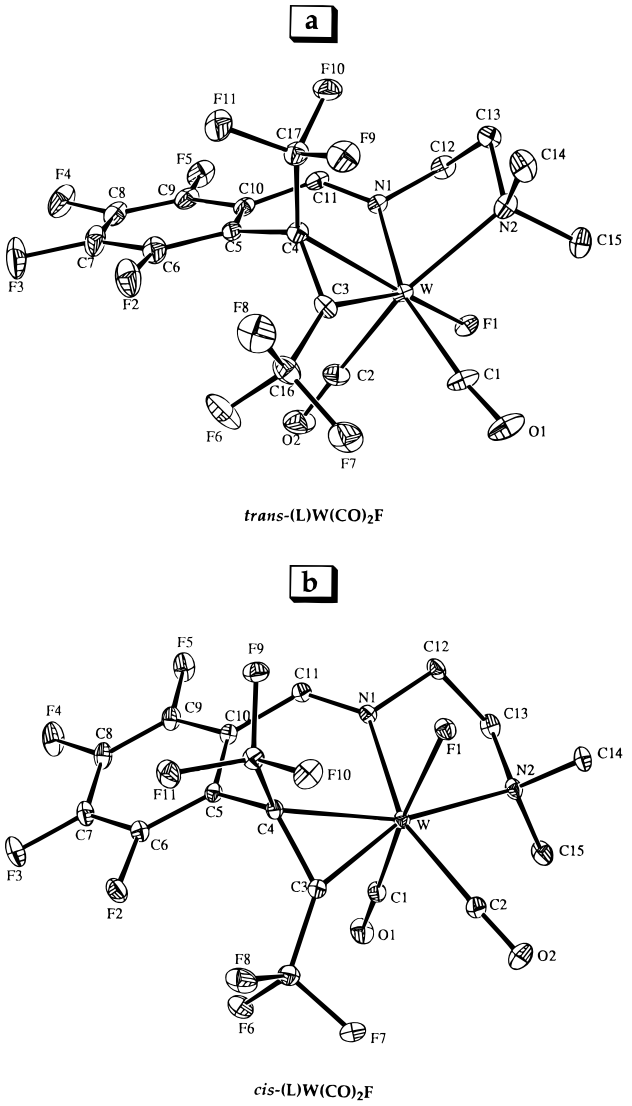


**Figure 2.** (a) ORTEP representation of **3**. (b) ORTEP representation of **4**.

constant for one of the carbonyl ligands at $\delta$ 221.79 ppm ($^2J_{CF}$ = 55 Hz) which clearly demonstrates that the ligand is *trans* to the fluoride.[24] The other carbonyl ligand at $\delta$ 221.82 ppm is *cis* to the fluoride with $^2J_{CF}$ = 5 Hz.[24] The structure of **4** was confirmed by X-ray crystallography (Figure 2b).[2]

The $^1$H NMR and the $^{19}$F NMR spectra for **4** are essentially identical to those of **3**. One notable peculiarity in the $^{19}$F NMR for **4** is that the W−F resonance was located unusually downfield as a singlet at $\delta$ −138.27 ppm. Its identity of the W−F resonance was ascertained by noting an upfield shift to $\delta$ −140.24 ppm upon addition of $D_2O$ to the sample.[19]

**X-ray Crystallographic Analyses of *trans*-{(L)W(CO)$_2$(F)} (3) and *cis*-{(L)W(CO)$_2$(F)} (4).** The structures of both $\eta^2$-vinyl complexes were confirmed by X-ray crystallography. Data collection information, positional parameters, selected bond distances, and bond angles for **3** and **4** are presented in Tables 1−4.

There exist several prominent structural features for $\eta^2$-vinyl complexes: (1) The orientations of the two $C_\beta$ substituents are roughly orthogonal to the $MC_\alpha C_\beta$ plane. (2) There are short M−$C_\alpha$ distances (1.92−1.96 Å) in the metal−carbon double bond range. (3) The M−$C_\beta$ distances (2.19−2.30 Å) are in the metal−carbon single-bond range. (4) $C_\alpha$−$C_\beta$ bond distances are suggestive of double-bond character.[5] For both compounds **3** and **4**, comparable crystallographic data were obtained supporting their formulation as $\eta^2$-vinyl complexes. In compounds **3** and **4**, the plane defined by the two $C_\beta$ substituents labeled C5 and C17 is roughly orthogonal to the $WC_\alpha C_\beta$ (W−C3−C4) plane as shown by the $R_\alpha$−$C_\alpha$−$C_\beta$−$R_\beta$ torsional angles in both the kinetic $\eta^2$-vinyl complex **3** (C16−C3−C4−C5 = −69.9° and C16−C3−C4−C17 = 74.1°) and the thermodynamic $\eta^2$-vinyl complex **4** (C16−C3−C4−C5 = 72.4° and C16−C3−C4−C17 = −75.0°). In addition, the sp$^3$ hybridization of the $C_\beta$ carbon is elucidated upon examination of the C−C−R and R−C−R bond angles at the four-coordinate carbon center in **3** (C5−C4−C17 = 110.1°, C3−C4−C5 = 122.0°, C3−C4−C17 = 119.0°, and C3−C4−W = 60.4°) and **4** (C5−C4−C17 = 111.2°, C3−C4−C5 = 121.8°, C3−C4−C17 = 119.6°, and C3−C4−W = 60.2°). Thus, the approximate tetrahedral angles at $C_\beta$ in both

**Table 1. Crystallographic Data for *trans*-(L)W(CO)$_2$(F) (3) and *cis*-(L)W(CO)$_2$(F) (4·$^1/_2$C$_7$H$_8$)**

| | **3** | **4** |
|---|---|---|
| molecular formula | $WF_{11}O_2N_2C_{17}H_{11}$ | $WF_{11}O_2N_2C_{17}H_{11}\cdot {}^1/_2C_7H_8$ |
| mol weight, g mol$^{-1}$ | 668.122 | 714.195 |
| space group | *Pbca* (No. 61) | $P\bar{1}$ (No. 2) |
| cryst system | orthorhombic | triclinic |
| cell constants | $a$ = 12.902(3) Å<br>$b$ = 16.185(2) Å<br>$c$ = 19.089(3) Å | $a$ = 8.100(1) Å<br>$b$ = 12.111(3) Å<br>$c$ = 12.944(4) Å<br>$\alpha$ = 100.69(2)°<br>$\beta$ = 97.92(3)°<br>$\gamma$ = 107.97(2)° |
| $V$, Å$^3$ | 3985.98 | 1160.79 |
| $Z$ | 8.0 | 2.0 |
| calcd density, g cm$^{-3}$ | 2.227 | 2.043 |
| cryst dimens, mm$^3$ | 0.42 × 0.39 × 0.19 | 0.32 × 0.25 × 0.15 |
| abs coeff ($\mu$), cm$^{-1}$ | 60.363 | 51.819 |
| radiation, $\lambda$(Mo K$\alpha$), Å | 0.709 30 | 0.709 30 |
| no. of reflcns measd | 2410 | 4384 |
| 2$\theta$ range, deg | 4.00−50.00 | 4.00−50.00 |
| scan technique: | $\theta$/2$\theta$ scan | $\theta$/2$\theta$ scan |
| scan width, deg | 0.8000 + 0.3400(tan $\theta$) | 0.8000 + 0.3400(tan $\theta$) |
| data collcn posn | bisecting, $\omega$ = 0 | bisecting, $\omega$ = 0 |
| decay corr appl | none | anisotropic |
| abs corr | empirical | empirical |
| min % transm | 40.6145 | 46.4511 |
| max % transm | 99.7504 | 99.9931 |
| av % transm | 76.2845 | 79.3357 |
| highest peak in diff Fourier map, e Å$^{-3}$ | 1.499 | 0.477 |
| max $\Delta\rho$ value in diff Fourier map, e Å$^{-3}$ | 2987.965 | 565.267 |
| ignorance factor, $p$ | 0.04 | 0.04 |
| no. of observns, $I > 3.00\sigma(I)$ | 2409 | 3700 |
| no. of variables | 299 | 385 |
| data to param ratio | 8.057 | 9.610 |
| shift to error ratio | 0.003 | 0.021 |
| error in an observn of unit weight | 0.9683 | 0.8023 |
| $R$ | 0.0378 | 0.0207 |
| $R_w$ | 0.0411 | 0.0266 |

[a] Relevant expressions are as follows, where $F_o$ and $F_c$ represent respectively the observed and calculated structure factor amplitudes. $R(F_o) = \Sigma(|F_o| - |F_c|/\Sigma|F_o|)$. $R_w(F_o) = [\Sigma(|F_o| - |F_c|)^2/\Sigma_w|F_o|^2]^{1/2}$.

(24) (a) Blake, A. J.; Cockman, R. W.; Ebsworth, E. A. V.; Holloway, J. H. *J. Chem. Soc., Chem. Commun.* **1988**, 529−530. (b) Darensbourg, D. J.; Klausmeyer, K. K.; Reibenspies, J. H. *Inorg. Chem.* **1995**, *34*, 4933−4934.

**Table 2. Atomic Coordinates and Equivalent Isotropic Thermal Parameters (Å²) for *trans*-(L)W(CO)₂(F) (3)**

| atom | *x* | *y* | *z* | *B*[a] (Å²) |
|---|---|---|---|---|
| W | 0.22744(3) | 0.00666(2) | 0.05482(2) | 2.957(7) |
| F1 | 0.1314(5) | −0.0742(4) | 0.0100(4) | 4.3(1) |
| F2 | 0.2849(7) | 0.1828(5) | 0.2468(4) | 8.0(2) |
| F3 | 0.1353(8) | 0.2642(6) | 0.3119(4) | 10.5(3) |
| F4 | −0.0493(7) | 0.2944(5) | 0.2457(5) | 9.5(2) |
| F5 | −0.0823(6) | 0.2316(5) | 0.1178(5) | 7.3(2) |
| F6 | 0.3343(7) | 0.0254(7) | 0.2478(4) | 9.6(3) |
| F7 | 0.4262(6) | −0.0531(5) | 0.1830(4) | 7.4(2) |
| F8 | 0.4658(6) | 0.0768(6) | 0.1966(5) | 8.2(2) |
| F9 | 0.4342(5) | 0.1627(5) | 0.0576(5) | 6.4(2) |
| F10 | 0.3005(6) | 0.2239(4) | 0.0188(4) | 5.6(2) |
| F11 | 0.3566(6) | 0.2536(5) | 0.1186(4) | 7.2(2) |
| O1 | 0.3723(7) | −0.1477(5) | 0.0638(6) | 7.4(3) |
| O2 | 0.1138(8) | −0.0522(6) | 0.1899(6) | 7.8(3) |
| N1 | 0.1135(6) | 0.0928(5) | 0.0124(5) | 3.3(2) |
| N2 | 0.2754(6) | 0.0219(5) | −0.0599(5) | 4.0(2) |
| C1 | 0.3176(9) | −0.0928(6) | 0.0651(8) | 4.9(3) |
| C2 | 0.156(1) | −0.0298(8) | 0.1401(7) | 5.2(3) |
| C3 | 0.3196(8) | 0.0490(7) | 0.1272(5) | 3.5(2) |
| C4 | 0.2727(8) | 0.1236(6) | 0.1062(6) | 3.4(2) |
| C5 | 0.1834(9) | 0.1611(6) | 0.1451(6) | 3.6(2) |
| C6 | 0.196(1) | 0.1904(8) | 0.2116(7) | 5.7(3) |
| C7 | 0.119(1) | 0.2337(8) | 0.2464(8) | 7.0(3) |
| C8 | 0.025(1) | 0.2473(8) | 0.2139(7) | 6.3(3) |
| C9 | 0.010(1) | 0.2167(7) | 0.1496(7) | 5.2(3) |
| C10 | 0.0875(8) | 0.1734(6) | 0.1152(6) | 3.7(2) |
| C11 | 0.0659(8) | 0.1505(6) | 0.0420(7) | 4.1(3) |
| C12 | 0.0972(8) | 0.0823(7) | −0.0625(7) | 4.7(3) |
| C13 | 0.2074(9) | 0.0861(7) | −0.0952(6) | 4.4(3) |
| C14 | 0.3846(9) | 0.0531(9) | −0.0715(7) | 5.7(3) |
| C15 | 0.265(1) | −0.0570(8) | −0.1004(7) | 5.6(3) |
| C16 | 0.3862(9) | 0.0263(9) | 0.1889(6) | 5.2(3) |
| C17 | 0.3387(9) | 0.1891(7) | 0.0764(6) | 4.4(3) |

[a] *B* values for anisotropically refined atoms are given in the form of the isotropic equivalent displacement parameter defined as (4/3)[$a^2\beta_{11} + b^2\beta_{22} + c^2\beta_{33} + ab(\cos\gamma)\beta_{12} + ac(\cos\beta)\beta_{13} + bc(\cos\alpha)\beta_{23}$].

**Table 3. Atomic Coordinates and Equivalent Isotropic Thermal Parameters (Å²) for *cis*-(L)W(CO)₂(F) (4·½C₇H₈)**

| atom | *x* | *y* | *z* | *B*[a] (Å²) |
|---|---|---|---|---|
| W | 0.90123(2) | 0.91343(2) | 0.72005(1) | 2.375(3) |
| F1 | 0.8542(4) | 0.9492(2) | 0.5767(2) | 3.43(6) |
| F2 | 0.5061(4) | 0.5373(3) | 0.7425(3) | 4.63(8) |
| F3 | 0.5993(5) | 0.3479(3) | 0.7547(3) | 5.98(9) |
| F4 | 0.8952(5) | 0.3281(3) | 0.6905(4) | 7.1(1) |
| F5 | 1.1052(4) | 0.5056(3) | 0.6218(3) | 5.83(9) |
| F6 | 0.5880(5) | 0.7427(3) | 0.8994(2) | 4.93(8) |
| F7 | 0.5732(5) | 0.9133(3) | 0.8901(3) | 5.43(8) |
| F8 | 0.3907(4) | 0.5749(3) | 0.7763(3) | 5.30(9) |
| F9 | 0.6453(4) | 0.6777(3) | 0.4765(2) | 4.15(7) |
| F10 | 0.5079(4) | 0.7878(3) | 0.5469(3) | 4.66(8) |
| F11 | 0.4301(4) | 0.6027(3) | 0.5493(3) | 4.74(8) |
| O1 | 1.0481(6) | 0.8828(4) | 0.9466(3) | 5.6(1) |
| O2 | 0.7715(6) | 1.1210(3) | 0.8242(4) | 5.6(1) |
| N1 | 1.0581(5) | 0.8249(3) | 0.6357(3) | 2.89(8) |
| N2 | 1.1716(5) | 1.0685(4) | 0.7431(3) | 3.31(9) |
| C1 | 0.9976(7) | 0.8953(5) | 0.8640(4) | 3.6(1) |
| C2 | 0.8171(7) | 1.0459(4) | 0.7892(4) | 3.6(1) |
| C3 | 0.6868(6) | 0.8180(4) | 0.7562(4) | 2.8(1) |
| C4 | 0.7004(6) | 0.7334(4) | 0.6656(4) | 2.65(9) |
| C5 | 0.7628(6) | 0.6303(4) | 0.6802(4) | 2.8(1) |
| C6 | 0.6597(7) | 0.5368(4) | 0.7145(4) | 3.4(1) |
| C7 | 0.7047(8) | 0.4365(5) | 0.7211(5) | 4.1(1) |
| C8 | 0.8540(8) | 0.4270(4) | 0.6878(5) | 4.5(1) |
| C9 | 0.9595(7) | 0.5179(5) | 0.6535(5) | 4.0(1) |
| C10 | 0.9186(6) | 0.6211(4) | 0.6493(4) | 3.0(1) |
| C11 | 1.0462(6) | 0.7147(4) | 0.6152(4) | 3.2(1) |
| C12 | 1.2005(6) | 0.9111(4) | 0.6021(4) | 3.7(1) |
| C13 | 1.2966(7) | 1.0126(5) | 0.7003(5) | 4.2(1) |
| C14 | 1.1512(8) | 1.1579(4) | 0.6805(5) | 4.1(1) |
| C15 | 1.2550(9) | 1.1361(6) | 0.8564(5) | 5.3(2) |
| C16 | 0.5611(7) | 0.8076(5) | 0.8293(4) | 3.6(1) |
| C17 | 0.5740(6) | 0.7020(4) | 0.5615(4) | 3.2(1) |
| C18 | 1.000(2) | 0.4079(8) | 2.0174(8) | 9.9(3) |
| C19 | 0.770(3) | 0.463(2) | 2.048(2) | 10.4(7) |
| C20 | 0.865(3) | 0.390(2) | 2.044(2) | 8.9(6) |
| C21 | 0.720(4) | 0.517(2) | 2.041(2) | 14.(1) |
| C22 | 0.896(2) | 0.506(1) | 2.018(1) | 7.2(5) |
| C23 | 1.144(3) | 0.427(2) | 1.997(2) | 18.4(8) |
| H1 | 1.140(9) | 0.695(6) | 0.565(6) | 5.0 |
| H2 | 0.873(9) | 1.068(6) | 0.471(6) | 5.0 |
| H3 | 1.275(9) | 0.876(6) | 0.566(6) | 5.0 |
| H4 | 1.347(9) | 0.972(6) | 0.747(6) | 5.0 |
| H5 | 1.429(9) | 1.081(6) | 0.682(6) | 5.0 |
| H6 | 1.267(9) | 1.216(6) | 0.682(6) | 5.0 |
| H7 | 0.915(9) | 0.888(6) | 0.408(6) | 5.0 |
| H8 | 1.057(9) | 1.192(6) | 0.700(6) | 5.0 |
| H9 | 1.396(9) | 1.182(6) | 0.860(6) | 5.0 |
| H10 | 1.271(9) | 1.068(6) | 0.901(6) | 5.0 |

[a] *B* values for anisotropically refined atoms are given in the form of the isotropic equivalent displacement parameter defined as (4/3)[$a^2\beta_{11} + b^2\beta_{22} + c^2\beta_{33} + ab(\cos\gamma)\beta_{12} + ac(\cos\beta)\beta_{13} + bc(\cos\alpha)\beta_{23}$]. All hydrogen atoms were located and refined except for those of the toluene.

compounds are inconsistent with an $\eta^1$-vinyl structure where M, $C_\alpha$, $C_\beta$, and the two $C_\beta$ constituents would lie in a plane.[25] In the kinetic $\eta^2$-vinyl complex **3**, W−$C_\alpha$ (W−C3) has a bond distance of 1.95(1) Å, W−$C_\beta$ (W−C4) has a bond distance of 2.21(1) Å, and $C_\alpha$−$C_\beta$ (C3−C4) definitely has double-bond character with a bond distance of 1.41(1) Å. Similarly, for the thermodynamic $\eta^2$-vinyl complex **4**, W−$C_\alpha$ (W−C3) has a bond distance of 1.938(5) Å, W−$C_\beta$ (W−C4) has a bond distance of 2.196(5) Å, and the double-bond character of $C_\alpha$−$C_\beta$ (C3−C4) is reflected in the bond distance of 1.448(7) Å. Also noteworthy is that in both **3** and **4** the sum of the angles around $C_\alpha$(C3) adds up to 360° as expected for an $sp^2$ center with no pyramidalization.

The geometry around the tungsten(II) metal center in both compounds can be described as roughly octahedral if one considers that the $\eta^2$-vinyl ligand occupies a single coordination site. The key structural difference between the kinetic $\eta^2$-vinyl complex **3** and the thermodynamic $\eta^2$-vinyl complex **4** is the relative orientation of the inserted alkyne to the other ligands around the tungsten(II) metal center. In **3**, the alkyne is roughly *trans* to the fluoride (F1−W−C3 = 156.1(3)° and F1−W−C4 = 156.4(4)°) and *cis* to the two carbonyl ligands (F1−W−C1 = 82.8(4)°, F1−W−C2 = 82.8(4)° and C3−W−C4 = 38.9(5)°). In contrast, the inserted alkyne in **4** is *cis* to the fluoride (F1−W−C3 = 112.3(2)°, F1−W−C4 = 92.7(2)°, and C3−W−C4 = 40.4(2)°) and one carbonyl ligand (F1−W−C2 = 91.0(2)°) and *trans* to the second carbonyl ligand (F1−W−C1 = 168.8(2)°). These structural variations not only seem to produce marked differences in reactivities of **3** and **4** but also appear to affect the solid-state packing of the molecules.

A survey of the packing in the unit cell shows that the complex **4** crystallizes as infinite chains of head-to-tail dimers linked by an C12−H···F1−W interaction (Supporting Information). The C12···F1 separation of 3.17 Å with a C12−H−F1 angle of 145° is consistent with weak intermolecular hydrogen bonding.[26] The

(25) Allen, S. R.; Baker, P. K.; Barnes, S. G.; Bottrill, M.; Green, M.; Orpen, A. G.; Welch, A. J. *J. Chem. Soc., Dalton Trans.* **1983**, 927−939.

(26) (a) Green, R. D. *Hydrogen Bonding by C-H Groups*; Wiley: New York, 1974; Chapter 5. (b) Desiraju, G. R. *J. Chem. Soc., Chem. Commun.* **1990**, 454−455. (c) Desiraju, G. R. *Acc. Chem. Res.* **1991**, *24*, 290−296.

**Table 4. Selected Distances (Å) and Angles (deg) for *trans*-(L)W(CO)$_2$(F) (3) and *cis*-(L)W(CO)$_2$(F) (4)[a]**

| | 3 | 4 |
|---|---|---|
| W−F1 | 1.994(6) | 1.996(3) |
| W−N1 | 2.182(9) | 2.178(4) |
| W−N2 | 2.29(1) | 2.342(5) |
| W−C1 | 2.00(1) | 1.996(6) |
| W−C2 | 1.96(1) | 2.037(6) |
| W−C3 | 1.95(1) | 1.938(5) |
| W−C4 | 2.21(1) | 2.196(5) |
| C3−C4 | 1.41(1) | 1.448(7) |
| F1−W−C1 | 82.8(4) | 168.8(2) |
| N1−W−C2 | 100.7(4) | 160.1(2) |
| N2−W−C3 | 118.4(4) | 158.2(2) |
| N2−W−C4 | 105.1(4) | 159.1(2) |
| C3−W−C4 | 38.9(5) | 40.4(2) |
| C3−C4−C17 | 119.(1) | 119.6(5) |
| C4−C3−C16 | 133.(1) | 132.3(5) |
| C3−C4−C5 | 122.(1) | 121.8(5) |
| W−C4−C5 | 111.3(6) | 116.5(3) |
| W−C4−C17 | 126.7(9) | 118.8(4) |
| W−C3−C16 | 144.9(9) | 148.2(4) |
| C5−C4−C17 | 110.1(9) | 111.2(5) |
| N2−W−C2 | 162.5(5) | 84.5(2) |
| N1−W−C1 | 160.8(4) | 94.6(2) |
| F1−W−C4 | 156.4(4) | 92.7(2) |
| F1−W−C3 | 156.1(3) | 112.3(2) |
| F1−W−C2 | 82.4(5) | 91.0(2) |
| C1−W−C2 | 87.0(6) | 91.3(3) |
| C2−W−C3 | 78.6(5) | 80.2(2) |
| C3−C4−W | 60.4(5) | 60.2(3) |
| C1−W−C3 | 81.9(6) | 78.9(2) |
| C16−C3−C4−C5 | −69.93(1.60) | 72.36(0.73) |
| C16−C3−C4−C17 | 74.05(1.57) | −74.99(0.70) |
| W−C4−C5−C10 | −50.69(1.15) | 47.44(0.55) |
| C4−C5−C10−C11 | −0.18(1.53) | −8.82(0.74) |
| C5−C10−C11−N1 | 28.36(1.56) | −19.27(0.80) |
| C10−C11−N1−W | 4.42(1.50) | 1.58(0.75) |
| C11−N1−W−C4 | −39.82(0.92) | 25.87(0.44) |
| N1−W−C4−C5 | 55.36(0.69) | −45.45(0.33) |

[a] Numbers in parentheses are estimated standard deviations in the least significant digits.

C12−N···F1 interaction has a distance of 2.15 Å which is shorter than the H···F van der Waals contact separation of 2.6 Å.[27] The basicity of the fluoride was further confirmed by the $^{19}$F NMR signal at $\delta$ −138.27 ppm which is slightly solvent dependent and shifts to $\delta$ −140.24 ppm upon addition of $D_2O$ to the sample suggesting hydrogen bonding to the fluoride.[19] In contrast, **3** does not exhibit hydrogen bonding in the solid state or in solution. This could be a result of the steric environment about the fluoride in **3** which is essentially encased by the ethylene ligand backbone (see Figure 2a), but the fluoride in **4** is accessible for intermolecular hydrogen bonding (see Figure 2b).

**Isotopic Enrichment of *trans*-{(L)W(CO)$_2$(F)} (3) and *cis*-{(L)W(CO)$_2$(F)} (4).** $^{13}$CO-labeled compounds were prepared in an effort to learn more about the $\eta^2$-vinyl systems as well as corroborate the $^{13}$C{$^{19}$F} NMR experiments. Isotopic exchange at 70 °C gave equal incorporation of $^{13}$CO into all three carbonyl positions in **6** and was confirmed by $^{13}$C{$^1$H} NMR spectroscopy which revealed equally intense $^{13}$CO enhanced carbonyl signals at $\delta$ 232.55 ppm ($^2J_{CF}$ = 41 Hz, $^1J_{CW}$ = 116 Hz), 221.58 ppm ($^2J_{CF}$ = 14 Hz, $^1J_{CW}$ = 132 Hz), and 218.76 ppm ($^2J_{CF}$ = 6 Hz, $^1J_{CW}$ = 122 Hz).

Using the same methods as those listed above for the preparation of **3** and **4**, the $^{13}$CO-enriched kinetic $\eta^2$-vinyl complex **7** ($\nu_{CO}$ 2047, 2021, 2001, 1966, 1946, 1928 cm$^{-1}$) and the $^{13}$CO-labeled thermodynamic $\eta^2$-vinyl complex **8** ($\nu_{CO}$ 2021, 1992, 1976, 1921, 1909, 1883 cm$^{-1}$) were prepared. Incorporation of $^{13}$CO into both carbonyl positions in **7** and **8** was confirmed by $^{13}$C{$^1$H} NMR spectroscopy which revealed equally intense $^{13}$CO enhanced carbonyl signals at $\delta$ 214.9 ppm ($^2J_{CF}$ = 20 Hz, $^1J_{CW}$ = 184 Hz) and 215.2 ppm ($^2J_{CF}$ = 13 Hz, $^1J_{CW}$ = 136 Hz) and $\delta$ 221.79 ppm ($^2J_{CF}$ = 55 Hz, $^1J_{CW}$ = 150 Hz) and 221.82 ppm ($^2J_{CF}$ = 5 Hz, $^1J_{CW}$ = 142 Hz), respectively.

**Synthesis and Characterization of *cis*-{(L)W(CO)(F)(P(OCH$_3$)$_3$)} (5).** Treatment of a toluene solution of **3** with 5 equiv of P(OMe)$_3$ at ambient temperature for 15 h affords a magenta solution of **5** ($\nu_{CO}$ 1953 cm$^{-1}$) which was isolated as a magenta microcrystalline solid in 59% yield from $Et_2O$/hexanes. NMR spectroscopy provided a wealth of structural information for the isotopically enriched P(OMe)$_3$-substituted $\eta^2$-vinyl complex which contains four different spin $^1/_2$ nuclei ($^{19}$F, $^{31}$P, $^{13}$C, $^{183}$W) in close proximity. The $^{31}$P{$^1$H} spectrum reveals a doublet of quartets for the coordinated P(OMe)$_3$ at $\delta$ 146.25 ppm with $^2J_{PF}$ = 81 Hz and $^1J_{PW}$ = 621 Hz. Likewise, the $^{19}$F NMR shows a doublet for W−F at $\delta$ −177.49 ppm with $^2J_{PF}$ = 81 Hz. P(OMe)$_3$ is also coupled to the trifluoromethyl group attached to the alkylidene carbon with a $^4J_{PF}$ = 8 Hz. This long-range interaction is also evident in the $^{19}$F NMR spectrum of **5** since the trifluoromethyl resonance appears as a doublet of doublets with $^4J_{PF}$ = 8 Hz from the trimethyl phosphite ligand and a remarkable $^6J_{FF}$ = 27 Hz from the *ortho* fluorine on the aromatic ring. The latter coupling is probably a "through-space" interaction which is not uncommon in other highly fluorinated systems.[28] In fact, previous work from this group has demonstrated that the fluorine *ortho* to the tungsten center in structurally related complexes readily engages in long-range interactions with other nuclei in the metallacycle.[29]

The large $^2J_{PF}$ coupling constant suggests a *trans* orientation between the fluoride and the phosphite ligands around the tungsten metal center. In the $^{13}$C{$^1$H} spectrum, the CO resonance appears as a pair of doublets at $\delta$ 235.60 ppm with $^2J_{CF}$ = 12 Hz, $^2J_{CP}$ = 7 Hz, and $^1J_{CW}$ = 146 Hz. The carbonyl coupling constants were unambiguously ascertained upon selective irradiation at the W−F $^{19}$F NMR resonance at $\delta$ −177.49 ppm which results in the collapse of the CO doublets to one doublet with $^2J_{CP}$ = 7 Hz. The small $^2J_{CF}$ carbonyl coupling constant indicates a *cis* orientation between the carbonyl and fluoride ligands.[24] The carbon resonances belonging to the $\eta^2$-vinyl fragment were not visible in the $^{13}$C{$^1$H} NMR spectrum due to the extensive coupling. Irradiation at the $CF_3(C_\alpha)$ $^{19}$F NMR resonance at $\delta$ −51.14 ppm results in the collapse of the quartet to a singlet at $\delta$ 131.46 ppm and the appearance of the $C_\alpha$ resonance as a pair of doublets centered at $\delta$ 189.45 ppm. Likewise, irradiation at the $CF_3(C_\beta)$ $^{19}$F NMR resonance at $\delta$ −55.93 ppm results in the collapse of the quartet to a singlet at $\delta$ 133.20 ppm for the trifluoromethyl group and the appearance of the $C_\beta$ resonance as a doublet centered at $\delta$ 31.28 ppm. The



(27) Bondi, A. *J. Phys. Chem.* **1964**, *68*, 441−451.

(28) (a) Servis, K. L.; Fang, K. N. *J. Am. Chem. Soc.* **1968**, *90*, 6712−6717. (b) Servis, K. L.; Jerome, F. R. *J. Am. Chem. Soc.* **1971**, *93*, 1535−1537. (c) Mallory, F. B.; Mallory, C. W.; Ricker, W. M. *J. Org. Chem.* **1985**, *50*, 457−461.

(29) Benn, R.; Rufińska, A.; King, M. A.; Osterberg, C. E.; Richmond, T. G. *J. Organomet. Chem.* **1989**, *376*, 359−366.

source of the additional couplings to $C_\alpha$ and $C_\beta$ could not be unequivocally ascertained.

Modeling studies[30] suggest that a *trans* orientation of the fluoride and $P(OCH_3)_3$ ligands is sterically favored relative to the *cis* orientation. Furthermore, the $^{13}C\{^{19}F\}$ NMR studies suggest that the trifluoromethyl moiety attached to the alkylidene carbon and the methyl groups on the trimethyl phosphite ligand are in close proximity. The $^{13}C\{^{1}H\}$ NMR spectrum displays the $P(OCH_3)_3$ ligand methyl resonances as an apparent quartet at $\delta$ 52.61 ppm and a doublet of doublets at $\delta$ 52.19 ppm with $^2J_{CP} = 7$ Hz and $^4J_{CF} = 3$ Hz. Thus, the methyl groups on the trimethyl phosphite ligand are not chemically equivalent. The different chemical shifts and coupling pattern reflect some sort of steric congestion preventing free rotation of the $P(OCH_3)_3$ ligand. The $^{13}C\{^{19}F\}$ NMR spectra are quite illustrative and present a more enigmatic coupling pattern for the $\delta$ 52.19 ppm doublet of doublets which when fully coupled appears as a complex quartet ($^1J_{CH} = 146$ Hz) of doublet of doublets resulting from coupling of the methyl moiety to the phosphorus atom and the tungsten fluoride ligand. Similarly, the apparent quartet at $\delta$ 52.19 ppm becomes quite intricate and emerges as a quartet of multiplets ($^1J_{CH} = 139$ Hz) resulting from coupling of the methyl fragment to not only the phosphorus atom and the tungsten fluoride but also the trifluoromethyl groups on the $\eta^2$-vinyl fragment as confirmed by numerous decoupling experiments.

The $^1$H NMR spectrum for **5** is analogous to those displayed by **3** and **4**. It is interesting that the imine proton is not affected by the increase in electron density at the tungsten center and emerges as a singlet at 8.82 ppm. Unlike the other $\eta^2$-vinyl complexes, the $^{19}$F NMR spectrum for **5** is quite interesting due to the presence of the trimethyl phosphite ligand on the tungsten metal. The resonances for the trifluoromethyl groups emerge as a singlet at $\delta$ −55.93 ppm and as a doublet of doublets at $\delta$ −51.14 ppm ($^4J_{PF} = 8$ Hz and $^6J_{FF} = 27$ Hz) which integrate to three fluorines each. The couplings due to the trimethyl phosphite and *ortho* fluorine ($\delta$ −131.35 ppm) on the tetrafluoroaryl group were determined from the aforementioned decoupling experiments. The aromatic fluorines appear as highly coupled multiplet resonances at $\delta$ −142.89, −149.70, and −159.04 ppm, and the W−F resonance is located farthest upfield as a doublet at $\delta$ −177.49 ppm ($^2J_{PF} =$ 81 Hz) due to coupling from the *trans* $P(OMe)_3$.

**Isomerization Kinetic Studies.** The $\eta^2$-vinyl isomerization shown in eq 2 proceeds readily at or above 60 °C in toluene solution. Photolysis of a toluene solution of **3** results in decomposition of the complex rather than isomerization. The IR spectral changes as a function of time for eq 2 at 70 °C are illustrated in Figure 3a. Isosbestic points are maintained at 2037, 2000, and 1936 cm$^{-1}$. Both the disappearance of **3** as well as the appearance of **4** gave identical rate constants within experimental error.

Interestingly, the $\eta^2$-vinyl isomerization of **3** exhibits a 20−30% rate enhancement in the presence of CO ([CO] ~ $9 \times 10^{-3}$ M).[31] As shown in Figure 4, the rate increases linearly with $p$(CO) which suggests the two-

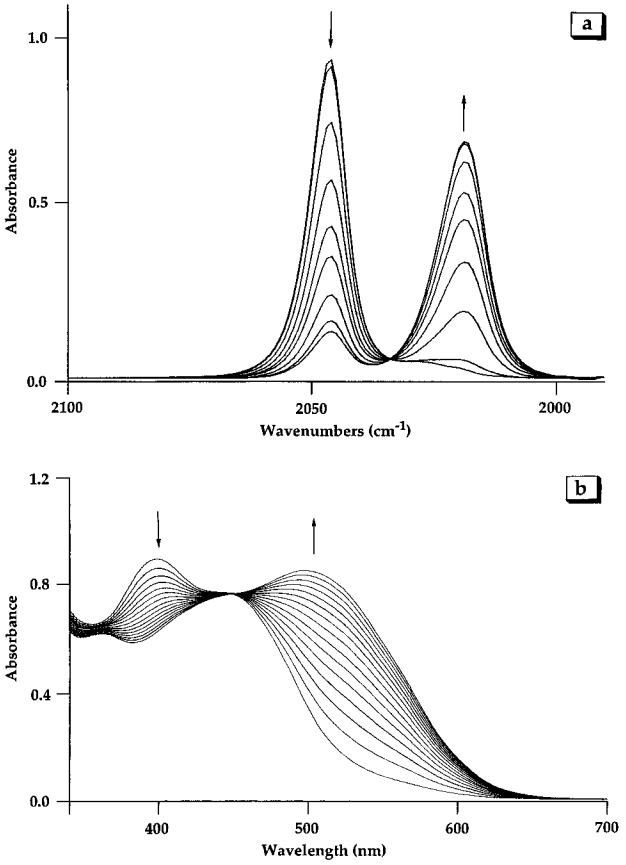


**Figure 3.** (a) Infrared spectral changes as a function of time for the $\eta^2$-vinyl isomerization of $2.55 \times 10^{-3}$ M **3** in toluene at 70 °C. (b) Visible spectral changes as a function of time ($\Delta t = 600$ s) for the reaction between $2 \times 10^{-4}$ M **3** and 0.21 M $P(OMe)_3$ at 25 °C and 100 atm.

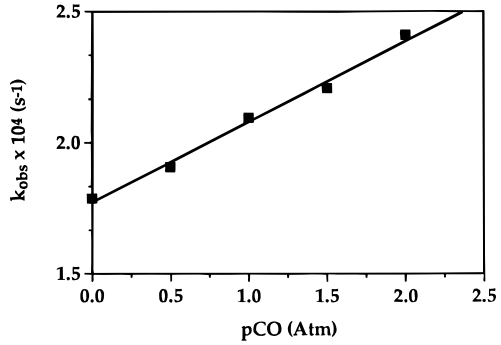


**Figure 4.** Plot of $k_{obs}$ (s$^{-1}$) versus CO concentration (M) for the $\eta^2$-vinyl isomerization of **3** in toluene solution at 80 °C.

term rate law described in eq 10. The observed rate

$$\frac{-d[3]}{dt} = k_1[3] + k_2[CO][3] \qquad (10)$$

constants for the spontaneous and CO-promoted $\eta^2$-vinyl isomerizations as a function of temperature and external pressure (0−100 MPa) are collected in Tables 5 and 6, respectively. Figure 5 illustrates the pressure dependence of the isomerization in the absence and presence of CO.

The activation parameters, $\Delta H^\ddagger = +124(\pm 2)$ kJ/mol, $\Delta S^\ddagger = +48(\pm 5)$ J/(mol·K), and $\Delta V^\ddagger = +15.6(\pm 0.4)$ cm$^3$/mol, were determined for the ligand-independent process (see Tables 5 and 6). The ligand-dependent process

(30) CAChe Worksystem 3.0 (CAChe Scientific, Beaverton, OR).
(31) Henry's law constant (221.47 L·atm·mol$^{-1}$) obtained from: Lühring, P.; Schumpe, A. *J. Chem. Eng. Data* **1989**, *34*, 250−252.

**Table 5. Observed Rate Constants, Activation Enthalpies, and Activation Entropies for the Spontaneous, CO-Promoted, and $P(OMe)_3$-Promoted $\eta^2$-Vinyl Isomerization as a Function of Temperature**

| [ligand], M | *T*, °C | rate const[a] | $\Delta H^{\ddagger}$, kJ mol$^{-1}$ | $\Delta S^{\ddagger}$, J mol$^{-1}$ K$^{-1}$ |
|---|---|---|---|---|
| no CO | | $k_1$, s$^{-1}$ | | |
| | 60 | $0.868 \times 10^{-4}$ | $124 \pm 2$ | $+48 \pm 5$ |
| | 70 | $3.106 \times 10^{-4}$ | | |
| | 80 | $11.200 \times 10^{-4}$ | | |
| | 90 | $37.700 \times 10^{-4}$ | | |
| CO, 0.009 | | $10^2 k_2$, M$^{-1}$ s$^{-1}$ | | |
| | 60 | $0.182 \times 10^{-2}$ | $98 \pm 3$ | $-5 \pm 9$ |
| | 70 | $0.461 \times 10^{-2}$ | | |
| | 80 | $1.330 \times 10^{-2}$ | | |
| | 90 | $3.610 \times 10^{-2}$ | | |
| $P(OMe)_3$, 0.20 | | $kK$, M$^{-1}$ s$^{-1}$ | | |
| | 20 | $6.608 \times 10^{-4}$ | $90 \pm 7$ | $+1 \pm 24$ |
| | 24.5 | $9.145 \times 10^{-4}$ | | |
| | 30 | $19.117 \times 10^{-4}$ | | |
| | 40 | $70.505 \times 10^{-4}$ | | |
| $P(OMe)_3$, 1.98 | | $k$, s$^{-1}$ | | |
| | 10 | $1.281 \times 10^{-4}$ | $77 \pm 2$ | $-46 \pm 6$ |
| | 20 | $4.012 \times 10^{-4}$ | | |
| | 24.5 | $6.398 \times 10^{-4}$ [b] | | |
| | 30 | $11.510 \times 10^{-4}$ | | |
| | 40 | $33.575 \times 10^{-4}$ | | |

[a] Determined by IR spectroscopy. [b] Determined by UV−vis spectroscopy.

**Table 6. Observed Rate Constants and Activation Volumes for the Spontaneous, CO-Promoted, and $P(OMe)_3$-Promoted $\eta^2$-Vinyl Isomerizations**

| [ligand], M | *P*, MPa | rate const[a] | $\Delta V^{\ddagger}$, cm$^3$ mol$^{-1}$ |
|---|---|---|---|
| no CO[b] | | $10^4 k_1$, s$^{-1}$ | |
| | 5 | $2.40 \pm 0.34$ | $+15.6 \pm 0.4$ |
| | 25 | $2.11 \pm 0.24$ | |
| | 50 | $1.82 \pm 0.10$ | |
| | 75 | $1.60 \pm 0.13$ | |
| | 100 | $1.40 \pm 0.13$ | |
| CO, 0.009[b] | | $10^2 k_2$, M$^{-1}$ s$^{-1}$ | |
| | 5 | $0.216 \pm 0.037$ | $+3.9 \pm 0.2$ |
| | 25 | $0.210 \pm 0.026$ | |
| | 50 | $0.202 \pm 0.011$ | |
| | 75 | $0.197 \pm 0.014$ | |
| | 100 | $0.188 \pm 0.015$ | |
| $P(OMe)_3$, 0.21[c] | | $10^4 k_{obs}$, s$^{-1}$ | |
| | 10 | $1.87 \pm 0.01$ | $+15.7 \pm 0.6$ |
| | 50 | $1.40 \pm 0.02$ | |
| | 100 | $1.04 \pm 0.07$ | |
| | 150 | $0.76 \pm 0.02$ | |
| $P(OMe)_3$, 2.22[c] | | $10^4 k_{obs}$, s$^{-1}$ | |
| | 10 | $6.8 \pm 0.2$ | $+5.5 \pm 0.4$ |
| | 50 | $6.0 \pm 0.2$ | |
| | 100 | $5.47 \pm 0.04$ | |
| | 150 | $4.9 \pm 0.2$ | |

[a] Rate constants are the mean values of at least three kinetic runs. [b] Kinetic runs performed at 60 °C. [c] Kinetic runs performed at 25 °C.

appears to be first order in added CO with activation parameters $\Delta H^{\ddagger} = +98(\pm 3)$ kJ/mol, $\Delta S^{\ddagger} = -5(\pm 9)$ J/(mol·K), and $\Delta V^{\ddagger} = +3.9(\pm 0.2)$ cm$^3$/mol (Tables 5 and 6). A complete listing of observed rate constants as a function of ligand concentration is available as Supporting Information.

Solutions of both **3** and **4** are indefinitely stable in the dark at ambient temperature under a nitrogen atmosphere. The thermodynamic isomer **4** is substitution inert and thermally robust. Treatment of a toluene solution of $^{13}$CO-labeled **4** with 2 atm of $^{12}$CO at 60 °C does not result in loss of the $^{13}$CO label. However, the

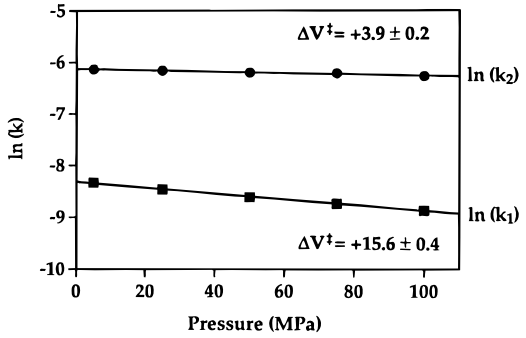


**Figure 5.** Pressure dependence of the $\eta^2$-vinyl isomerization for a $2 \times 10^{-4}$ M toluene solution of **3** at 60.1 °C in the absence of CO (■) and in the presence of 0.009 M CO (●).

kinetic isomer **3** is substitution labile as determined by both IR and NMR spectroscopic techniques. Specifically, treatment of a toluene solution of $^{13}$CO-labeled **3** with 2 atm of $^{12}$CO at ambient temperature results in loss of the $^{13}$CO label and uptake of CO by **3** upon conversion to **4**. Importantly, treatment of a toluene-$d_8$ solution of **3** with 1 atm of $^{13}$CO at 80 °C for 10 min results in approximately 50% isomerization (with incorporation of $^{13}$CO upon conversion to **4**) and uptake of the $^{13}$CO label by **3** in accord with a dissociative process. Treatment of **3** with *tert*-butyl isonitrile does not promote the $\eta^2$-vinyl isomerization but instead leads to degradation of **3** presumably due to attack of the imine functionality of **3** by the nucleophilic isonitrile. The substitution inert **4** does not react with *tert*-butyl isonitrile, CO, or $P(OMe)_3$.

The $\eta^2$-vinyl isomerization is, however, promoted by $P(OMe)_3$, and the kinetics of this process were investigated. As depicted in eq 11, treatment of a toluene

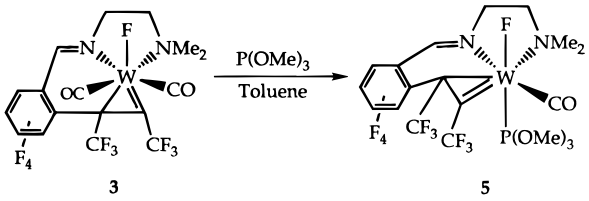


(11)

solution of **3** with $P(OMe)_3$ at or above room temperature affords **5** in which the $P(OMe)_3$ is *trans* to the fluoride and the inserted acetylene is *cis* to the fluoride. The isomerization reaction was monitored by observing changes in the visible spectra as a function of time as illustrated in Figure 3b. Again, excellent agreement was obtained with rates determined by infrared spectroscopy. The yellow color of the starting material is replaced by the intense magenta color of the $P(OMe)_3$-substituted product, and isosbestic points (360 and 452 nm) are maintained throughout the course of the transformation. Upon extended reaction times and high [$P(OMe)_3$], a small amount of secondary reactivity of this complex is observed and results in some formation of the disubstituted phosphite complex as well as decomposition products. The formation of the bis(phosphite) complex was ascertained by the diagnostic $^{19}$F NMR doublet of doublet resonance at $\delta$ −186.68 ppm ($^2J_{PF}$ = 73 Hz and $^2J_{PP}$ = 43 Hz). The repetitive scan spectra recorded under these conditions also have some deviations from that reported in Figure 3b.

The rate of eq 11 varies with the $P(OMe)_3$ concentration as well as with temperature and pressure. The

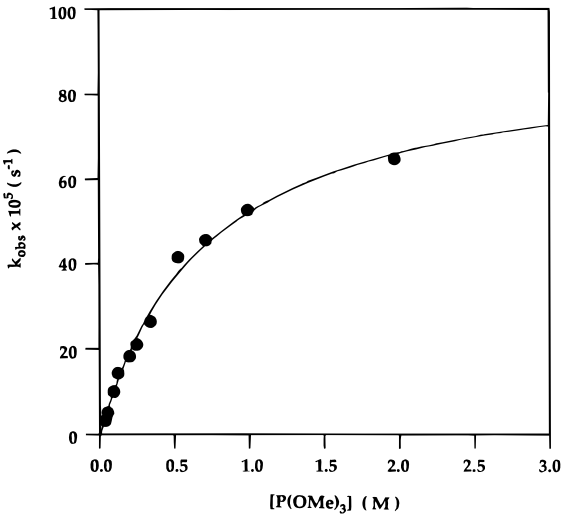


**Figure 6.** Plot of $k_{obs}$ ($s^{-1}$) versus $P(OMe)_3$ concentration (M) for the $\eta^2$-vinyl isomerization of $2 \times 10^{-4}$ M **3** in toluene solution at 25 °C.

**Scheme 2**

$$3 + P(OMe)_3 \underset{}{\overset{K}{\rightleftharpoons}} [3 \cdot P(OMe)_3] \qquad [3 \cdot P(OMe)_3] \xrightarrow{k} 5$$

reaction is first-order in the tungsten complex **3**. The $\eta^2$-vinyl isomerization process (eq 11) displays *saturation kinetics*, in which the reactivity tends toward a limiting value with increasing concentration of $P(OMe)_3$. Figure 6 illustrates this saturation behavior and shows $k_{obs}$ as a function of $[P(OMe)_3]$ at 25 °C. This behavior is typical of a mechanism involving the formation of an adduct as shown in Scheme 2 and described by eq 12.[32]

$$k_{obs} = \frac{K k [P(OMe)_3]}{1 + k [P(OMe)_3]} \qquad (12)$$

The concentration dependence of the reaction at low $[P(OMe)_3]$ (ca. 0.2 M) shows linear behavior and $k_2 = kK$. For high $[P(OMe)_3]$ (ca. 2 M), the limiting $k_{obs}$ value is in fact the rate constant $k$. The solid line in Figure 6 represents the least-squares fit of the data and gives $K = 1.4 \pm 0.1$ $M^{-1}$ and $k = (89 \pm 13) \times 10^{-5}$ $s^{-1}$, such that $kK = 1.2 \times 10^{-3}$ $M^{-1}$ $s^{-1}$.[33] The initial slope of the plot at low $[P(OMe)_3]$ has a value of $1.1 \times 10^{-3}$ $M^{-1}$ $s^{-1}$ which must represent $kK$ and is indeed close to that calculated from the values of $k$ and $K$ above. An error due to a change in the reaction medium upon mixing solutions of **3** and $P(OMe)_3$ can be excluded, since apparent association constants from medium effects are on the order of $\leq 0.1$ $M^{-1}$, which is significantly less than the $K$ value obtained in the present study.[34]

Spectra of solutions of **3** and $P(OMe)_3$ were recorded before and immediately after mixing in the tandem cuvette in an attempt to obtain evidence for the adduct [**3**·$P(OMe)_3$]. As shown in Figure 7, there is an instantaneous change in the spectrum, an absorbance decrease

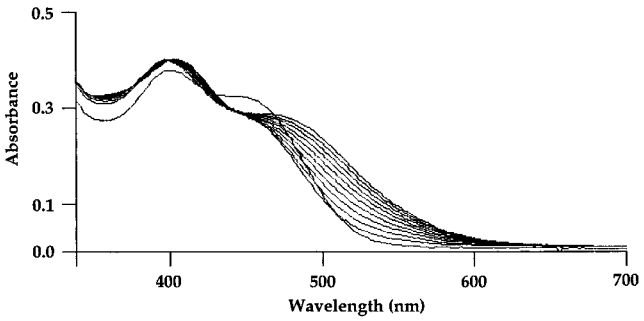


**Figure 7.** Repetitive scan spectra for the $P(OMe)_3$-promoted $\eta^2$-vinyl isomerization in toluene at 25 °C. Conditions: [**3**] = $2 \times 10^{-4}$ M; $[P(OMe)_3]$ = 2.20 M; first spectrum recorded before mixing using a tandem cuvette; subsequent spectra recorded at 100 s intervals.

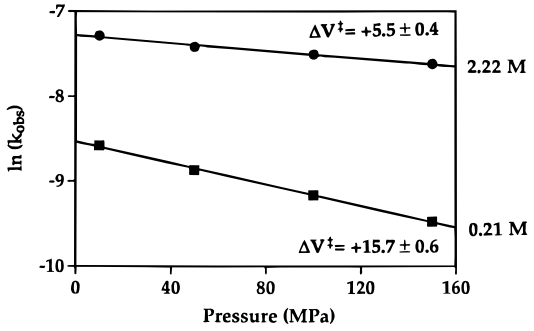


**Figure 8.** Pressure dependence of the $\eta^2$-vinyl isomerization for a $2 \times 10^{-4}$ M toluene solution of **3** at 25 °C in the presence of 0.21 M $P(OMe)_3$ (■) and in the presence of 2.22 M $P(OMe)_3$ (●).

at ca. 460 nm and an absorbance increase at ca. 400 nm, on mixing **3** and $P(OMe)_3$. Importantly, the extent of the spectral changes correlates directly with the $P(OMe)_3$ concentration employed. It follows that this spectral change must be due to the rapid formation of the adduct on mixing the two components. The complex possesses $\lambda_{max}$ at 400 nm and at 460 nm. The subsequent conversion to **5** is a clean process which exhibits a single isosbestic at $\lambda = 420$ nm as illustrated in the repetitive scan spectrum in Figure 7. Unfortunately, attempts to observe the adduct formation using variable-temperature NMR spectroscopy proved unsuccessful.

The observed rate constants for the $P(OMe)_3$-promoted $\eta^2$-vinyl isomerization as a function of temperature and pressure are reported in Tables 5 and 6. Figure 8 displays the pressure dependence of the isomerization in the presence of $P(OMe)_3$. At low trimethyl phosphite concentrations, the activation parameters $\Delta H^{\ddagger} = +90(\pm 7)$ kJ/mol, $\Delta S^{\ddagger} = +1(\pm 24)$ J/(mol·K), and $\Delta V^{\ddagger} = +15.7(\pm 0.6)$ $cm^3$/mol were determined for $kK$ (Tables 5 and 6). The activation parameters, $\Delta H^{\ddagger} = +77(\pm 2)$ kJ/mol, $\Delta S^{\ddagger} = -46(\pm 6)$ J/(mol·K), and $\Delta V^{\ddagger} = +5.5(\pm 0.4)$ $cm^3$/mol, were determined at high $[P(OMe)_3]$ for $k$ (Tables 5 and 6). A complete listing of observed rate constants as a function of ligand concentration is available as Supporting Information.

## Discussion

**Formation of $\eta^2$-Vinyl Complexes.** Although metal-mediated couplings of perfluoroalkenes and -alkynes are well precedented, simple insertion reactions in which

(32) (a) Bassetti, M.; Mannina, L.; Monti, D. *Organometallics* **1994**, *13*, 3293−3299. (b) Wax, M. J.; Bergman, R. G. *J. Am. Chem. Soc.* **1981**, *103*, 7028−7030. (c) Monti, D.; Bassetti, M. *J. Am. Chem. Soc.* **1993**, *115*, 4658−4664.

(33) Sigma Plot Version 1.02, Windows 3.10 Enhanced (Jandel Scientific, Corte Madera, CA).

(34) Beck, M. T. *Chemistry of Complex Equilibria*; Van Nostrand Reinhold: London, 1970; p 86.

**Scheme 3**

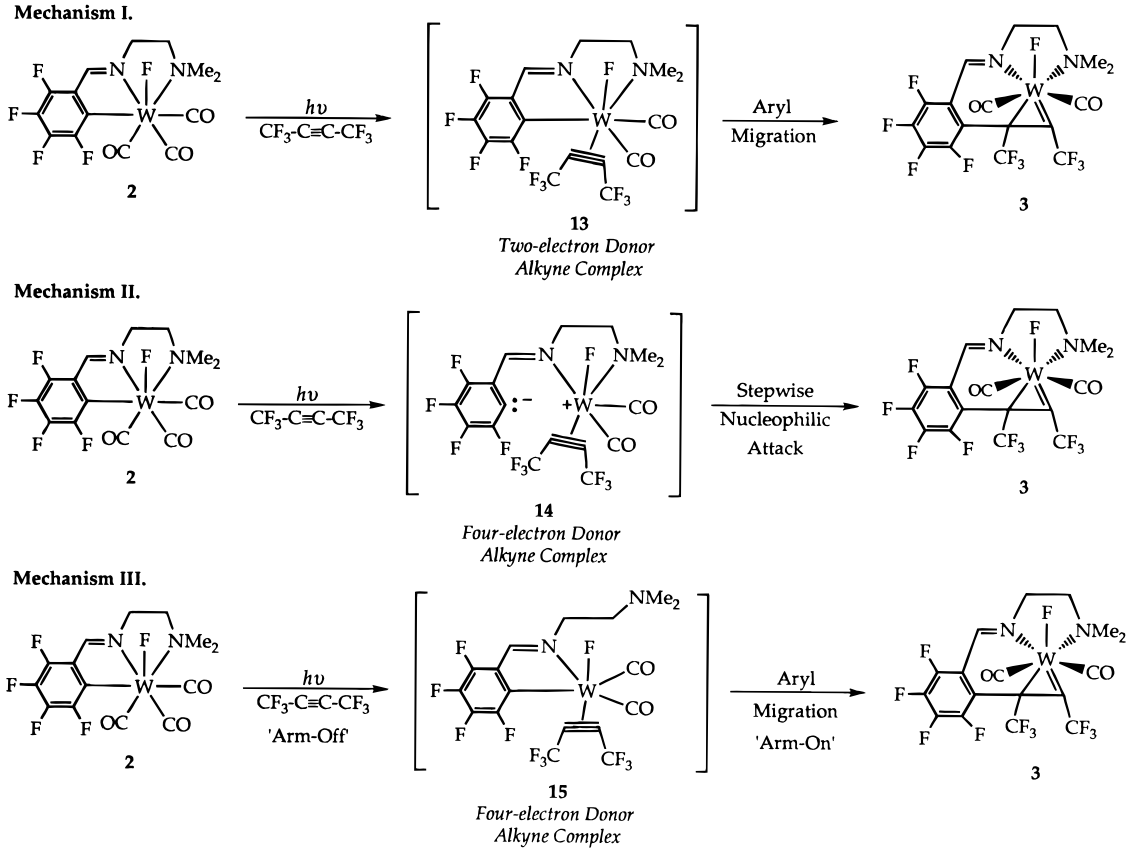


the migrating group is highly fluorinated are quite rare, presumably due to the increased strength and reduced nucleophilicity of the metal−carbon bond compared to those of hydrocarbon analogues.[35] The slightly shorter metal−$C_{Aryl}$ bond in **2** (2.207(4) Å)[36] compared to **10** (2.226(5) Å)[37] is consistent with this trend.

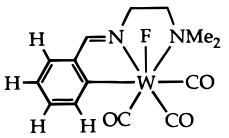

**10**

Indeed, it is remarkable that migration of the highly fluorinated metallacycle is facile at room temperature when a coordination site is made available by photolysis. Davidson and co-workers reported several examples of intramolecular nucleophilic attack on coordinated perfluoro-2-butyne to form novel $\eta^2$-vinyl complexes as depicted in eq 13.[12d,17] These reactions involve attack by lone pairs of coordinated ligands rather than the migratory insertion pathway discovered in the present work.[38]

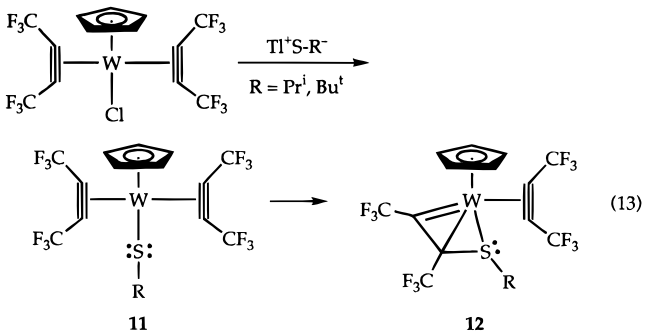


(13)

Thus, an attractive mechanistic rationale for the chemistry presented in this work involves initial CO loss from **2** followed by coordination of the acetylene to generate the $d^4$ alkyne complex **13**. As depicted in Scheme 3, this transient complex is an 18-electron system in which the hexafluoro-2-butyne serves as a *two-electron donor* ligand. Subsequent migration of the pendant tetrafluoroaryl group at the coordinated alkyne would then yield the kinetic $\eta^2$-vinyl complex **3**. It seems likely that the slow step in the thermal reaction sequence is loss of CO. This is substantiated by the important observation that isotopic incorporation of $^{13}CO$ into the parent compound **2** requires temperatures of at least 60 °C, which is the same temperature required for thermal production of **4**. The fast step appears to be the aryl migration since all spectroscopic attempts to detect complex **13** have proven unsuccessful.

The migration is certainly promoted by the electron-poor perfluorinated alkyne ligand since the $CF_3$ groups increase the electrophilicity of the alkyne carbons. Additionally, due to its inherent electron deficiency, hexafluoro-2-butyne resists functioning in a four-

(35) (a) Albéniz, A. C.; Espinet, P.; Jeannin, Y.; Philoche-Levisalles, M.; Mann, B. E. *J. Am. Chem. Soc.* **1990**, *112*, 6594−6600. (b) Albéniz, A. C.; Espinet, P.; Foces-Foces, C.; Cano, F. H. *Organometallics* **1990**, *9*, 1079−1085. (c) Albéniz, A. C.; Espinet, P. *Organometallics* **1991**, *10*, 2987−2988. (d) Gipson, S. L.; Kneten, K. *Inorg. Chim. Acta* **1989**, *157*, 143−145.

(36) Osterberg, C. E. Ph.D. Thesis, University of Utah, 1990.

(37) Kiplinger, J. L. Unpublished results (data to appear in an upcoming paper).

(38) For a related reaction involving $TlSC_5H_4N$ see: (a) Davidson, J. L.; Murray, I. E. P.; Preston, P. N.; Russo, M. V.; Manojlović-Muir, L.; Muir, K. W. *J. Chem. Soc., Chem. Commun.* **1981**, 1059−1061. (b) Davidson, J. L.; Murray, I. E. P.; Preston, P. N.; Russo, M. V. *J. Chem. Soc., Dalton Trans.* **1983**, 1783−1787.

electron donor capacity; it prefers to act as a two-electron donor.[5] In fact, Davidson and co-workers have observed similar intermolecular reactivity trends for bis(perfluoro-2-butyne) complexes with heteroatom nucleophiles.[12b−d,17,38b] The perfluorinated alkyne ligands not only act as "nucleophile magnets" but the resulting $\eta^2$-vinyl product showcases the second hexafluoro-2-butyne ligand residing as a two-electron donor.

An alternative mechanism would entail the heterolytic cleavage of the $W-C_{Aryl}$ bond to generate the species **14** in which the metal fragment is an 18-electron tungsten(II) cationic complex with hexafluoro-2-butyne serving as a four-electron donor ligand. As depicted in Scheme 3, this process can be considered as the intramolecular counterpart to the existing intermolecular nucleophilic additions reported for cationic $d^4$ alkyne complexes. The pendant tetrafluoroaryl group exists as a stabilized carbanion[39] and could then attack the alkyne carbons in an intramolecular fashion to yield **3**. In this capacity, hexafluoro-2-butyne encourages the conversion of the alkyne to its more electron-rich isolobal $\eta^2$-vinyl cousin.[40] However, it seems unlikely that the electron-deficient perfluorinated alkyne would serve as a four-electron donor ligand or even allow the formation of the cationic tungsten(II) complex **14**.

As illustrated in Scheme 3, a third possibility could involve the concomitant dechelation of the $NMe_2$ appendage with CO loss upon coordination of the alkyne to afford the dicarbonyl complex **15** in which hexafluoro-2-butyne serves as a four-electron donor ligand. Aryl migration followed by reattachment of the $NMe_2$ arm would then produce **3**. In fact, this sort of anchimeric assistance has recently been reported for ligand substitution reactions in square-planar iridium(I) and rhodium(I) complexes that incorporate the potentially terdentate monoanionic saturated [C,N,N′] ligand system $C_6H_4CH_2N(Me)CH_2CH_2NMe_2$-2.[41]

At a first glance, one notices an apparent difficulty associated with the first mechanism in that a two-electron donor alkyne ligand is not isolobal with a three-electron donor $\eta^2$-vinyl ligand. However, since the nucleophile source (and extra electrons) is derived from the metal−$C_{Aryl}$ bond upon migration it does accurately account for the observed reaction chemistry. Thus, we favor mechanism I although transient dissociation of the $NMe_2$ group ("arm-off−arm-on" process) is difficult to rule out.[42]

Photolysis appears to access the early portion of the reaction coordinate for the thermal reaction of **2** with hexafluoro-2-butyne, since the kinetic $\eta^2$-vinyl complex **3** is easily converted to the thermodynamic $\eta^2$-vinyl complex **4** at or above 60 °C. This provides strong evidence that **3** is indeed an intermediate in the formation of **4**. The isomerization is accompanied by a significant shift to lower energy in the carbonyl stretching frequencies ($\sim$50 $cm^{-1}$) which suggests the presence of greater electron density at the metal center for the thermodynamic $\eta^2$-vinyl product **4**. Due to steric problems associated with forcing the rigid tridentate $\eta^3$-[C,N,N′] imine ligand to assume a facial coordination mode, the kinetic $\eta^2$-vinyl complex **3** shows a greater distortion from octahedral geometry than does the thermodynamic $\eta^2$-vinyl isomer **4** (vide infra). Thus, the shift to lower stretching frequency simply could reflect an increase in the F p$\pi$ to metal d$\pi$ to CO $\pi^*$ back-bonding as a result of better orbital overlap between the metal and ligands upon isomerization.

The average CO stretching frequencies of **3** and **4** are greater than that of the tricarbonyl starting material **2** and suggest that the highly fluorinated $\eta^2$-vinyl ligand is a strong $\pi$-acceptor. It has been shown that hexafluoro-2-butyne is capable of acting as a more effective double-faced $\pi$-acid than carbon monoxide.[12b] Furthermore, it is also known that $\eta^2$-vinyl ligands are isolobal to four-electron donor acetylenes and use essentially the same orbitals in their interactions with metal centers.[40] Hence, it follows that the perfluorinated $\eta^2$-vinyl fragment generated in these complexes is also an effective $\pi$ acid.

As has been demonstrated through hydrogen bonding studies of related tungsten(II) fluoride carbonyl complexes, the $^{19}F$ NMR resonance of the fluoride bound to tungsten is quite sensitive to electronic effects.[19] Importantly, a decrease in the basicity of the fluoride ligand accompanies the isomerization as evidenced by a dramatic shift in the W−F resonance from $\delta$ −172.26 ppm for **3** to $\delta$ −138.27 ppm for **4** and a reduction in the tendency of W−F to engage in hydrogen bonding. This trend is strengthened by **2** which displays a $^{19}F$ NMR resonance at $\delta$ −223.38 ppm ($CDCl_3$) for W−F and also exhibits significant hydrogen bonding in both the solid state and solution.[19]

The $^{13}C\{^1H\}$ NMR spectra are also a decisive tool for identifying $\eta^2$-vinyl ligands. The carbenoid character of $C_\alpha$ in these complexes is reflected in large downfield chemical shifts.[22] Indeed, compounds **3**−**5** possess spectroscopic parameters compatible with other $d^4$ $\eta^2$-vinyl monomeric complexes as shown in Table 7. The use of $^{13}C\{^{19}F\}$ decoupling experiments in conjunction with the preparation of $^{13}CO$-labeled complexes elucidated several coupling interactions involving the perfluorinated $\eta^2$-vinyl moiety. Presumably a consequence of a strong F(p$\pi$)−W(d$\pi$)−$C_\alpha$(p$\pi$) orbital interaction in compound **3**, the alkylidene carbon unveiled a rather significant coupling of $^2J_{CF} = 34$ Hz to the *trans* fluoride. The presence of this interaction indicates that both the fluoride as well as the $\eta^2$-vinyl fragment retain coordination to the metal center in solution. The coupling of the $C_\beta$ carbon to the tungsten fluoride could not be resolved. Two carbonyl resonances were displayed at $\delta$ 215.24 ppm with $^2J_{CF} = 13$ Hz and $^1J_{CW} = 136$ Hz and at $\delta$ 214.97 ppm with $^2J_{CF} = 20$ Hz and $^1J_{CW} = 184$ Hz for the carbonyls *cis* to the fluoride. The tungsten bound fluoride also coupled to one methyl and one methylene carbon producing doublets with 4 and 6 Hz couplings, respectively.

For complex **4**, the coupling of $C_\alpha$ and $C_\beta$ could not be determined in accordance with a *cis* relationship with the metal fluoride. The two carbonyl resonances emerged at $\delta$ 221.82 ppm with $^2J_{CF} = 5$ Hz and $^1J_{CW} = 142$ Hz

(39) Cohen, S. C.; Massey, A. *Adv. Fluorine Chem.* **1970**, *6*, 83−285.

(40) Brower, D. C.; Birdwhistell, K. R.; Templeton, J. L. *Organometallics* **1986**, *5*, 94−98.

(41) Wehman-Ooyevaar, I. C. M.; Kapteijn, G. M.; Grove, D. M.; Smeets, W. J. J.; Spek, A. L.; van Koten, G. *J. Chem. Soc., Dalton Trans.* **1994**, 703−711.

(42) A similar process has been reported for five-coordinate chiral tin complexes that contain a bidentate C,N ligand: (a) van Koten, G.; Jastrzebski, J. T. B. H.; Noltes, J. G.; Pontenagel, W. M. G. F.; Kroon, J.; Spek, A. L. *J. Am. Chem. Soc.* **1978**, *100*, 5021−5028. (b) Jastrzebski, J. T. B. H.; Boersma, J.; van Koten, G. *J. Organomet. Chem.* **1991**, *413*, 43−53.

**Table 7. Relevant Structural and Spectroscopic Parameters for Molybdenum(II) and Tungsten(II) $\eta^2$-Vinyl Complexes[a]**

| complex | M=$C_\alpha$, Å | M−$C_\beta$, Å | $C_\alpha$−$C_\beta$, Å | $\delta(C_\alpha)$, ppm | $\delta(C_\beta)$, ppm | ref |
|---|---|---|---|---|---|---|
| CpMo[P(OMe)$_3$]$_2$($\eta^2$-CPhCHPh) | 1.95 | 2.30 | 1.43 | 255.5 | 26.8 | 9b,c |
| CpMo[P(OMe)$_3$]$_2$($\eta^2$-CBu$^t$CHPh) | 1.94 | 2.29 | 1.44 | 286.5 | 29.9 | 9c |
| CpMo[P(OMe)$_3$]$_2$($\eta^2$-CMeCPh$_2$) | 1.96 | 2.25 | 1.46 | 237.4 | 35.7 | 9c |
| ($\eta^5$-C$_9$H$_7$)Mo[P(OMe)$_3$]$_2$($\eta^2$-CSiMe$_3$CH$_2$) | 1.96 | 2.26 | 1.44 | 276.5 | 23.9 | 9a,c |
| CpMoCl(CF$_3$C≡CCF$_3$)[$\eta^2$-CF$_3$CC(CF$_3$)(PEt$_3$)] | 1.92 | 2.29 | 1.43 | N/A | N/A | 18 |
| CpMoCl(CF$_3$C≡CF$_3$)[$\eta^2$-CF$_3$CC(CF$_3$)(PEt$_3$)] | 1.91 | 2.32 | 1.42 | N/A | N/A | 18 |
| CpMo(CF$_3$C≡CCF$_3$)[$\eta^3$-CF$_3$CC(CF$_3$)(NC$_5$H$_4$S)] | 1.91 | 2.12 | 1.39 | N/A | N/A | 38a |
| [(Tp′)(CO)$_2$Mo($\eta^2$-CPh=CHCH=N(Me)(Bu$^t$)][BF$_4$] | 1.97 | 2.28 | 1.45 | 242.6 | 40.7 | 14 |
| CpW(CO)$_2$[$\eta^2$-CF$_3$CC(CF$_3$)(−C(=O)SMe)] | 1.96 | 2.19 | 1.44 | N/A | N/A | 60 |
| CpW(SC$_6$H$_4$CH$_3$)(CF$_3$C≡CCF$_3$)[$\eta^2$-CF$_3$CC(CF$_3$)(PEt$_3$)] | 1.91 | 2.33 | 1.45 | N/A | N/A | 12a |
| CpW(CF$_3$C≡CCF$_3$)[$\eta^3$-CF$_3$CC(CF$_3$)(SPr$^i$)] | 1.91 | 2.18 | 1.42 | N/A | N/A | 17 |
| CpWCl(CF$_3$C≡CCF$_3$)[$\eta^2$-CF$_3$CC(CF$_3$)(CNBu$^t$)] | 1.89 | 2.30 | 1.41 | N/A | N/A | 12a |
| (dtc)$_3$W($\eta^2$-CPh=CPhCPh=CHPh) | 1.94 | 2.32 | 1.43 | 260.6 | 62.1 | 13 |
| *trans*-(L)W(CO)$_2$(F) (**3**) | 1.95 | 2.21 | 1.41 | 196.8 | 32.4 | this work |
| *cis*-(L)W(CO)$_2$(F) (**4**) | 1.94 | 2.196 | 1.45 | 202.8 | 40.8 | this work |
| *cis*-(L)W(CO)(F)(P(OMe)$_3$) (**5**) | N/A | N/A | N/A | 189.5 | 31.3 | this work |

[a] N/A = data not available.

for the carbonyl *cis* to the fluoride and at $\delta$ 221.79 ppm with $^2J_{CF}$ = 55 Hz and $^1J_{CW}$ = 150 Hz for the carbonyl *trans* to the fluoride. The carbonyl *trans* to the fluoride showed the largest coupling constant. The tungsten bound fluoride also coupled to one methyl and one methylene carbon producing doublets with 15 and 3 Hz couplings, respectively.

Due to the presence of P(OMe)$_3$ in compound **5**, the $^2J_{CF}$ and $^2J_{CP}$ couplings to the $\eta^2$-vinyl ligand could not be resolved. However, the sole carbonyl ligand was observed at $\delta$ 235.60 ppm with $^2J_{CF}$ = 12 Hz, $^2J_{CP}$ = 7 Hz, and $^1J_{CW}$ = 146 Hz. The small couplings constants for these interactions provide compelling evidence for a *cis* orientation of the carbonyl ligand with the P(OMe)$_3$ and fluoride ligands.[43] Further evidence for the geometry about the tungsten(II) metal center is gleaned from the $^{19}$F NMR and $^{31}$P{$^1$H} NMR spectra which reveal a large $^2J_{PF}$ coupling constant of 81 Hz which strongly suggests a *trans* relationship between the fluoride ligand and the P(OMe)$_3$ ligand.[43] One point of interest is that the $^{13}$C{$^{19}$F} NMR data how that the trimethyl phosphite ligand appears to have restricted rotation as evidenced by the appearance of two methyl resonances at $\delta$ 52.61 ppm as an apparent quartet with $^1J_{CH}$ = 139 Hz (due to extensive C−P and C−F couplings the methyl carbon multiplets could not be resolved) and at $\delta$ 52.19 ppm with $^1J_{CH}$ = 146 Hz, $^2J_{CP}$ = 7 Hz, and $^4J_{CF}$ = 3 Hz. The restricted freedom of rotation of the trimethyl phosphite ligand was qualitatively confirmed through modeling studies.

The W−$C_\alpha$ coupling for the coordinated $\eta^2$-vinyl ligand which is frequently observed in tungsten(II) alkylidene complexes[8,13,23] was not discernible, presumably due to extensive fluorination in complexes **3**−**5**. The rigid structure of the $\eta^2$-vinyl products at room temperature is also illustrated by the $^{13}$C NMR data. Formation of $\eta^2$-vinyl ligands with two different $C_\beta$ substituents creates diastereotopic carbonyl ligands due to chirality at the $C_\beta$ carbon and the metal center. Because of the low symmetry of the molecule, the carbonyl carbons are going to be inequivalent regardless of the time scale of the $\eta^2$-vinyl rotation. Indeed, only one isomer is observed for compounds **3** and **4**. Although heating **3** generates **4** via the isomerization process discussed below, complex **4** is remarkably robust and exhibits no measurable fluxional processes up to 90 °C.

**Scheme 4**

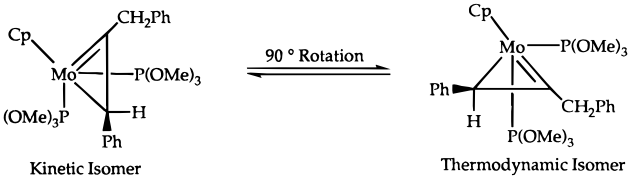


A single trifluoromethyl resonance would be anticipated for a dynamic $\eta^2$-vinyl process occurring in these complexes since rotation of the $\eta^2$-vinyl fragment would necessarily make the two $CF_3$ groups equivalent. Instead, two $CF_3$ resonances are observed in the $^{19}$F NMR spectra for the $\eta^2$-vinyl complexes **3**−**5**. Note that Green,[9c] Davidson,[12c−d,17,18] and Templeton[14] have observed a plethora of fluxional processes in their $\eta^2$-vinyl systems. Typically, some sort of windshield wiper type motion (less than or equal 90° rotation) of the $\eta^2$-vinyl fragment is invoked to explain the dynamic behavior in these systems as illustrated in Scheme 4. Thus, it is noteworthy that Green reported the isolation of two distinct $\eta^2$-vinyl isomers for the complex [CpMo[P(OMe)$_3$]$_2$($\eta^2$-C(CH$_2$Ph)CHPh)] which only differ in the orientation of the $\eta^2$-vinyl moiety.[9c] Presumably, the inherent steric constraints imposed by the rigid tridentate $\eta^3$-[C,N,N′] chelate ligand system prevent this classical windshield wiper motion from occurring (rotation of the $\eta^2$-vinyl ligand). Any dynamic process would require a disconnection/reconnection between $C_\beta$ and the aromatic carbon, which is highly unlikely. Hence, complexes **3**−**5** are static on the NMR time scale as expected for a six-coordinate complex.

In contrast to structurally similar later transition metal complexes, the $\eta^2$-vinyl complexes reported in this work are chemically robust toward multiple alkyne insertions into the W−$C_{aryl}$ bond. The later transition metal complexes readily undergo multiple insertion reactions with activated acetylenes to form large metallacycle complexes as well as heterocyclic ring systems upon metal extrusion.[44] In fact, a mechanism for Ziegler−Natta type alkyne polymerization based on $\eta^2$-vinyl intermediates has been proposed.[45] Thus, these tungsten(II) $\eta^2$-vinyl complexes could actually resemble a snapshot along the reaction path for alkyne insertion into a M−C bond.

(43) (a) Doherty, N. M.; Hoffman, N. W. *Chem. Rev.* **1991**, *91*, 553−573. (b) Simpson, R. D.; Bergman, R. G. *Organometallics* **1993**, *12*, 781−796.

The highly fluorinated $\eta^2$-vinyl complexes presented in this work are unique. Importantly, this work illustrates the distinctive reaction chemistry associated with metal fluoride compounds since the $\eta^2$-vinyl derivatives are not accessible from known tungsten(II) chloride complexes.[46]

**Solid−State Structures of the $\eta^2$-Vinyl Products.** Single-crystal X-ray studies unambiguously confirmed the molecular structures of the $\eta^2$-vinyl complexes **3** and **4**. Close examination revealed the structures to be remarkably similar (Table 4). Due to the relatively small C4−W−C3 bite angle of the $\eta^2$-vinyl moiety in compounds **3** (38.9(5)°) and **4** (40.4(2)°), the ligand can be considered as occupying a single coordination site such that the tungsten metal center adopts a pseudooctahedral geometry in these systems. Both complexes possess structural parameters in accord with the proposed metallacyclopropene framework (Table 7). Compound **3** has a short W−C3 bond distance of 1.95(1) Å which is consistent with a W=C double bond.[47] The W−C4 bond distance of 2.21(1) Å is in the range of a W−C single bond.[47] Furthermore, the C3−C4 bond clearly exhibits partial double-bond character with a bond length of 1.41(1) Å, justifying the proposed $\eta^2$-vinyl structure. The kinetic $\eta^2$-vinyl complex exhibits similar structural parameters with a W−C3 bond length of 1.938(5) Å, a W−C4 bond length of 2.196(5) Å, and a C3−C4 bond distance of 1.448(7) Å.

Molecular orbital studies regarding the $CpM(CO)_2$ fragment have shown that the preferred orientation for the $\pi$-acid $\eta^2$-vinyl fragment is perpendicular to the double-faced-$\pi$-acid carbonyl ligands. That is, the optimal orientation is such that the empty p orbital on the alkylidene carbon fragment will align itself antisymmetric with respect to the mirror plane which bisects the carbonyl ligands.[48] The three $\pi$-acids are *roughly* orthogonal to each other in both structures. However, upon isomerization the tungsten metal center better attains an octahedral geometry as shown by comparing the bond angles around tungsten in **3** (C1−W−C2 = 87.0(6)°; C2−W−C3 = 78.6(5)°; Cl−W−C3 = 81.9(6)°; C2−W−F = 82.4(5)°; C1−W−F = 82.8(4)°; C3−W−F = 156.1(3)°) with those in complex **4** (C1−W−C2 = 91.3(3)°; C2−W−C3 = 80.2(2)°; C1−W−C3 = 78.9(2)°; C2−W−F = 91.0(2)°; C1−W−F = 168.8(2)°; C3−W−F = 112.3(2)°). Thus, the geometry around tungsten for the thermodynamic $\eta^2$-vinyl complex is slightly more octahedral than for the kinetic $\eta^2$-vinyl complex. This would be expected so as to maximize overlap for bonding and hence minimize competition for metal d$\pi$ electron density. This is in agreement with the spectroscopic observations (vide supra).

The W−C1 and W−C2 bonds in **3** (2.00(1) and 1.96(1) Å) and **4** (1.996(6) and 2.037(6) Å) have typical W−C carbonyl bond lengths comparable to values reported for related tungsten(II) fluoride carbonyl complexes.[19,49] Interestingly, the W−F bond distance is essentially identical in both complexes **3** (1.994 Å) and **4** (1.996 Å) and does not appear to be strongly affected by the ligand *trans* to it. However, in both six-coordinate complexes the W−F bond is somewhat shorter than the 2.037(2) Å reported for the precursor seven-coordinate tungsten(II) fluoride complex **2**.[36] This is most likely a consequence of the highly fluorinated $\eta^2$-vinyl ligand which is electron-withdrawing and makes the metal center rather electron poor in comparison to complex **2**. In regards to $\sigma$ bonding, the fluoride ligand would be expected to have a stronger bonding interaction with a less basic metal center, thus shortening the W−F bond distance. Furthermore, the amount of fluoride p$\pi$ to metal d$\pi$ donation would be expected to increase with a decrease in metal basicity and this in turn would result in a shortening of the metal−fluoride bond. Thus, in these tungsten(II) fluoride complexes the highly fluorinated $\eta^2$-vinyl, or cyclic alkylidene, fragment appears electrophilic enough to invoke $\pi$ donation from the fluoride ligand. This reduced electron density on the fluoride ligand could also justify the dramatic downfield shift observed for the W−F resonance in the $^{19}$F NMR spectra for **3** ($\delta$ −172.26 ppm) and **4** ($\delta$ −138.27 ppm) versus that reported for **2** ($\delta$ −214.60 ppm, acetone-$d_6$).

In both the structures of **3** and **4** the length of the W−N1 bond in the five-membered metallacycle is significantly shorter than the W−N2 bond (Table 4). This can also be readily explained using the metal−ligand $\pi$ overlap argument. An increase in the metal−ligand $\pi$ interaction results in an increase in bond order and a decrease in the metal−ligand bond length. Thus, the imine N1 atom with $sp^2$ hybridization (sum of angles around N1 in both complexes is 360°) is expected to have a greater bonding interaction and shorter bond lengths than the $sp^3$-hybridized N2 atom. It is noteworthy to mention that the W−N1 bond in **4** (2.342(5) Å) which is *trans* to the $\eta^2$-vinyl fragment is significantly longer than the W−N1 bond in **3** (2.29(1) Å) which is *trans* to a carbonyl ligand. This implies a stronger *trans* influence for the perfluorinated $\eta^2$-vinyl ligand relative to a carbonyl ligand. The strong *trans* influence for alkylidene ligands has been noted by others.[50]

Thus, it would appear that a cummulative effect of many subtle differences in sterics and electronics between the two structures perhaps best rationalizes why the isomerization occurs. The insertion of the hexafluoro-2-butyne into the $W-C_{Aryl}$ bond generates a six-membered tungstenacycle which is not planar in either complex. This is in contrast with five-membered metallacycles, such as that contained within the tungsten(II) complex **2**, which are planar presumably due to extensive delocalization of $\pi$ electron density throughout metallacycle.[51] Examination of the torsional angles within and surrounding the six-membered metallacycle

(44) (a) Maassarani, F.; Pfeffer, M.; Le Borgne, G. *Organometallics* **1987**, *6*, 2029−2043. (b) Wu, G.; Rheingold, A. L.; Heck, R. F. *Organometallics* **1986**, *5*, 1922−1924. (c) Bahsoun, A.; Dehand, J.; Pfeffer, M.; Zinsius, M.; Bouaoud, S. E.; Le Borgne, G. *J. Chem. Soc., Dalton Trans.* **1979**, 547−556. (d) Arlen, C.; Pfeffer, M.; Fischer, J.; Mitschler, A. *J. Chem. Soc., Chem. Commun.* **1983**, 928−929.

(45) Carlton, L.; Davidson, J. L.; Ewing, P.; Manojlović-Muir, L.; Muir, K. *J. Chem. Soc., Chem. Commun.* **1985**, 1474−1476.

(46) (a) Richmond, T. G.; King, M. A.; Kelson, E. P.; Arif, A. M. *Organometallics* **1987**, *6*, 1995−1996. (b) Poss, M. J.; Arif, A. M.; Richmond, T. G. *Organometallics* **1988**, *7*, 1669−1670.

(47) Churchill, M. R.; Youngs, W. J. *Inorg. Chem.* **1979**, *18*, 2454−2458.

(48) Schilling, B. E. R.; Hoffmann, R.; Lichtenberger, D. L. *J. Am. Chem. Soc.* **1979**, *101*, 585−591.

(49) Kiplinger, J. L.; Arif, A. M.; Richmond, T. G. *Inorg. Chem.* **1995**, *34*, 399−401.

(50) (a) Birdwhistell, K. R.; Nieter Burgmayer, S. J.; Templeton, J. L. *J. Am. Chem. Soc.* **1983**, *105*, 7789−7790. (b) Appleton, T. G.; Clark, H. C.; Manzer, L. E. *Coord. Chem. Rev.* **1973**, *10*, 335−422. (c) Shustorovich, E. M.; Porai-Koshits, M. A.; Buslaev, Y. A. *Coord. Chem. Rev.* **1975**, *17*, 1−98.

(51) (a) Bruce, M. I. *Angew. Chem., Int. Ed. Engl.* **1977**, *16*, 73−86. (b) Richmond, T. G.; Osterberg, C. E.; Arif, A. M. *J. Am. Chem. Soc.* **1987**, *109*, 8091−8092.

**Scheme 5**

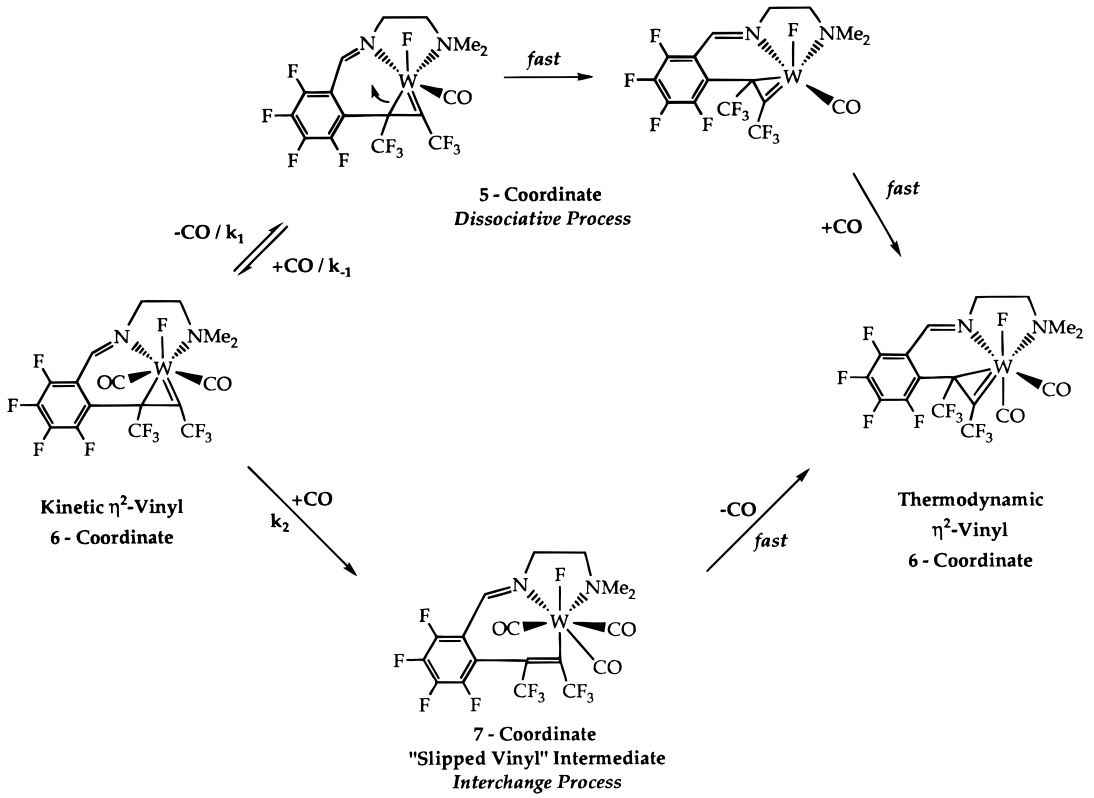


in each structure shows a larger deviation from planarity for the tungstenacycle in **3** (W−C4−C5−C10, −50.7°; C4−C5−C10−C11, −0.2°; C5−C10−C11−N1, 28.4°; C1−C11−N1−W, 4.4°; C11−N1−W−C4, −39.8°; N1−W−C4−C5, 55.4°) than in **4** (W−C4−C5−C10, 47.4°; C4−C5−C10−C11, −8.8°; C5−C10−C11−N1, −19.3°; C1−C11−N1−W, 1.6°; C11−N1−W−C4, 25.9°; N1−W−C4−C5, −45.5°). The greater distortion from planarity in **3** most likely stems from the fact that the monoanionic $\eta^3$-[C,N,N′] chelate ligand fragment (defined earlier as L) is forced into an unfavorable facial arrangement in **3** whereas the tridentate chelate binds to the tungsten center in a meridional manner in **4**. These two distinct bonding arrangements for the tridentate ligand can be gleaned from the N2−W−C4−C5 torsional angle of 127.2°, the N2−W−C4 bond angle of 105.1°, and the N2−W−C3 bond angle of 118.4° in **3** versus a N2−W−C4−C5 torsional angle of −47.0°, a N2−W−C4 bond angle of 159.1°, and a N2−W−C3 angle of 158.2° in **4**.

In seven-coordinate tungsten(II) complexes with a capped octahedral geometry, the phenyl carbon of the monoanionic $\eta^3$-[C,N,N′] chelating imine ligand caps an octahedral face rather than binds in a strictly meridional or facial manner.[19,46,49] In contrast, recent reports have demonstrated that the saturated tridentate monoanionic $\eta^3$-[C,N,N′] amine ligand, which can be considered as the more flexible cousin of the unsaturated imine ligand, can readily attain and typically favors a facial binding array in stereochemically similar tungsten(II) carbonyl complexes.[52] The intense strain inflicted upon the rigid $\eta^3$-[C,N,N′] imine ligand in confining the ligand to coordination in a strictly meridional fashion is perhaps best illustrated by the facile addition of acetone to the imine of **16** to afford **17** in which the tridentate monoanionic $\eta^3$-[C,N,N′] ligand is coordinated to the metal center in a facial manner (eq 14).[53]

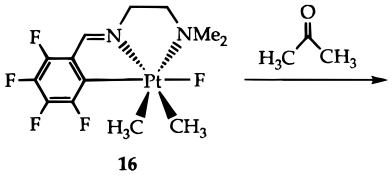

**16**

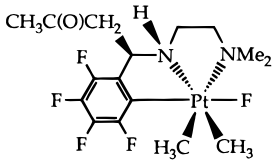

**17** (14)

**Kinetics and Mechanism of the $\eta^2$-Vinyl Isomerization.** The kinetics and mechanisms of ligand substitution reactions of octahedral metal carbonyl complexes comprises a vast body of research and has been the subject of several reviews.[54] The $\eta^2$-vinyl isomerization process follows the two-term rate law given in eq 10. This suggests that a competitive dual pathway mechanism is operative as is illustrated in Scheme 5.

The $k_1$ term is a first−order process with respect to the disappearance of the tungsten complex **3**. The large positive volume of activation (+15.6 cm$^3$ mol$^{-1}$) and entropy of activation (+48 J mol$^{-1}$ K$^{-1}$) suggest that a

(52) (a) Buffin, B. P.; Arif, A. M.; Richmond, T. G. *J. Chem. Soc., Chem. Commun.* **1993**, 1432−1434. (b) Buffin, B. P.; Poss, M. J.; Arif, A. M.; Richmond, T. G. *Inorg. Chem.* **1993**, *32*, 3805−3806.

(53) (a) Anderson, C. M.; Puddephatt, R. J.; Ferguson, G.; Lough, A. J. *J. Chem. Soc., Chem. Commun.* **1989**, 1297−1298. (b) Anderson, C. M.; Crespo, M.; Ferguson, G.; Lough, A. J. *Organometallics* **1992**, *11*, 1177−1181.

(54) (a) Basolo, F. *Polyhedron* **1990**, *9*, 1503−1535. (b) Darensbourg, D. J. *Adv. Organomet. Chem.* **1982**, *21*, 113−150. (c) Howell, J. A. S.; Burkinshaw, P. M. *Chem. Rev.* **1983**, *83*, 557−599.

limiting dissociative mechanism is operative. Dissociation of CO is the rate-determining step, followed by rapid isomerization and recombination with CO. An informative comparison is provided by the CO substitution reaction of $Cr(CO)_4$(phen) (phen = 1,10-phenanthroline) with $P(OMe)_3$ as the attacking nucleophile. It was determined that the reaction proceeds via a dissociative mechanism characterized by a large volume of activation ($+13.8 \pm 0.5$ cm$^3$ mol$^{-1}$) which is comparable to the value obtained for $k_1$.[55] Large positive volumes of activation in the range from 16 to 24 cm$^3$ mol$^{-1}$ have also been reported for the dissociation of CO from ruthenium cluster compounds of the type $[Ru_3(CO)_{10/11}]^-$.[56] Similarly, a dissociative mechanism was reported for the ring closure reaction of $Cr(CO)_5$(dab) (dab = 1,4-diisopropyl-1,4-diazabutadiene) with a $\Delta V^{\ddagger} = +17.2 \pm 1.0$ cm$^3$ mol$^{-1}$.[57] Also consistent with a dissociative process is the enthalpy of activation (124 kJ mol$^{-1}$) which is somewhat smaller than the M−CO bond dissociation values for other group VI metal carbonyl complexes.[58] In conjunction with the unusually high CO stretching frequencies of complex **3** (vide supra), the reduced W−CO bond energy could similarly be a consequence of the great $\pi$-acceptor ability of the perfluorinated $\eta^2$-vinyl ligand. The presence of the highly fluorinated $\eta^2$-vinyl ligand withdraws electron density from the metal center, reduces back-bonding, and weakens the W−CO bond, thus promoting a dissociative mechanism. *cis*-Labilization by fluoride may also promote CO loss.[59]

The $k_2$ term is a second-order process, with a small negative entropy of activation (−5 J mol$^{-1}$ K$^{-1}$) and a small positive volume of activation (+3.9 cm$^3$ mol$^{-1}$). Importantly, the enthalpy of activation for the $k_2$ term (98 kJ mol$^{-1}$) is significantly less than that for the $k_1$ process which is in accord with less bond breaking and more bond formation in the transition state. A direct comparison of the $\Delta S^{\ddagger}$ values for the $k_1$ and $k_2$ terms is not possible due to the different units of $k_1$ and $k_2$ that will affect the $\Delta S^{\ddagger}$ value. The CO-assisted isomerization reaction is clearly an intramolecular process. The near zero values for $\Delta S^{\ddagger}$ and $\Delta V^{\ddagger}$ imply that the reaction is intramolecular during which bond formation and breakage practically cancel each other in terms of volume and entropy changes. The first-order dependence of the rate on the CO concentration provides compelling evidence that an association of **3** with CO occurs to assist the isomerization process. This association can be visualized in terms of an interchange mechanism I during which bond formation and bond breakage contributions cancel each other in terms of volume and entropy effects. This would mean that attack by free CO and the subsequent release of coordinated CO occur in a concerted manner. Thus, an interchange (I) mechanism best rationalizes the CO-promoted $\eta^2$-vinyl isomerization process (eq 2).

**Scheme 6**

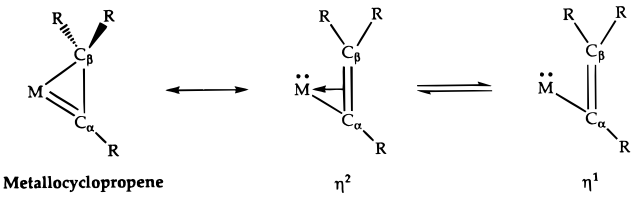


The dissociative pathway via a 16-electron intermediate is consistent with the 16/18-electron rule; the associative pathway involving a 20-electron intermediate is incongruous with this formalism. However, it has previously been suggested that the $\eta^2$-vinyl ligand can change its hapticity from $\eta^2$-to $\eta^1$ as depicted in Scheme 6.[38a,45,60] In such a manner, the $\eta^2$-vinyl ligand could conceivably accept a pair of electrons and the complex would then maintain an 18-electron count at the metal center during the associative pathway and thus avoid a 20-electron transition state. The well-known rate-enhancing ability of variable hapticity ligands (e.g indenyl,[61] nitrosyl[54a]) to dramatically enhance the rate of ligand substitution reactions suggests that this is a reasonable explanation. It is noteworthy that, unlike the static six-coordinate systems, both five-coordinate and seven-coordinate complexes are known to readily undergo nonrigid processes at the metal center.[62] Thus, the rearrangements depicted in Scheme 5 could rationalize the observed $\eta^2$-vinyl isomerization.

The tendency toward saturation is typical of a process that entails the formation of a kinetically detectable intermediate. Wax and Bergman[32b] observed saturation kinetics for the migratory CO insertion reaction of $CpMo(CO)_3(CH_3)$ in a series of methyl-substituted THF solvents which provided compelling evidence for solvent-assisted alkyl migration although they did not actually observe the solvent-coordinated intermediate. Recently, Monti and Bassetti[32a,c] reported the detection of a weak molecular iron−phosphine complex in the phosphine−induced migratory insertion reaction of $(\eta^5\text{-}C_9H_7)Fe(CO)_2(CH_3)$ which also exhibits saturation kinetics. Importantly, slippage of the indenyl ligand from $\eta^5$ to an $\eta^3$ mode was not invoked to allow for the association of the phosphine.

The greatest limitation imposed by CO-promoted kinetics was the inability to attain high enough solution concentrations to observe saturation.[63] As such, we chose to examine the kinetics of the $\eta^2$-vinyl isomerization reaction using the sterically similar trimethyl phosphite to achieve higher nucleophile concentrations. The reaction of the kinetic $\eta^2$-vinyl complex **3** with trimethyl phosphite clearly exhibits saturation kinetics as shown in Figure 6. The observed saturation kinetics is interpreted in terms of a rapid pre-equilibrium ($K$) during which the adduct species [**3**·$P(OMe)_3$] is formed, followed by a rate-determining step ($k$) to produce **5**, thus, providing compelling evidence for the existence of the mechanism proposed in Scheme 2. Direct evidence for the formation of the adduct was reported above (see Figure 7), and the treatment of the kinetic data



(55) Schneider, K. J.; van Eldik, R. *Organometallics* **1990**, *9*, 1235−1240.
(56) Taube, D. J.; van Eldik, R.; Ford, P. C. *Organometallics* **1987**, *6*, 125−129.
(57) Reddy, K. B.; van Eldik, R. *Organometallics* **1990**, *9*, 1418−1421.
(58) Simões, J. A. M.; Beauchamp, J. L. *Chem. Rev.* **1990**, *90*, 629−688.
(59) (a) Atwood, J. D.; Brown, T. L. *J. Am. Chem. Soc.* **1976**, *98*, 3160−3166. (b) Lichtenberger, D. L.; Brown, T. L. *J. Am. Chem. Soc.* **1978**, *100*, 366−373. (c) Hoffman, N. W.; Prokopuk, N.; Robbins, M. J.; Jones, C. M.; Doherty, N. M. *Inorg. Chem.* **1991**, *30*, 4177−4181.
(60) Davidson, J. L.; Shiralian, M.; Manojlović-Muir, L.; Muir, K. W. *J. Chem. Soc., Dalton Trans.* **1984**, 2167−2176.
(61) O'Connor, J. M.; Casey, C. P. *Chem. Rev.* **1987**, *87*, 307−318.
(62) Wilkins, R. G. *Kinetics and Mechanism of Reactions of Transition Metal Complexes*, 2nd ed.; VCH Publishers: New York, 1991.
(63) Wilhelm, E.; Battino, R. *Chem. Rev.* **1973**, *73*, 1−9.

suggested a formation constant of $1.4 \pm 0.1$ $M^{-1}$. This value is such that relatively high nucleophile concentrations have to be employed to achieve saturation. Naturally, this would not have been seen for the CO-assisted reaction at the low CO concentrations ($\leq 0.009$ M) used. Furthermore, the large difference in nucleophilicity between CO and $P(OMe)_3$ will strongly affect the value of $K$, which accounts for the large difference in the observed reactivities ($k_2[CO] \ll kK[P(OMe)_3]$). The value of $kK$ ($=1.1 \times 10^{-3}$ $M^{-1}$ $s^{-1}$) was taken from the initial slope at low $[P(OMe)_3]$ in Figure 6. The molecular nature of the precursor adduct [**3**·$P(OMe)_3$] could not be determined due to the interference of the subsequent reaction to produce **5**. The observed spectral changes during formation of the adduct suggest that $P(OMe)_3$ enters the coordination sphere of the complex **3** or at least binds to a coordinated ligand. By way of comparison, Basetti and co-workers[32a] observed equilibrium constants ranging from $K = 0.94$ to 8.0 $M^{-1}$ for the formation of [($\eta^5$-$C_9H_7$)$Fe(CO)_2(CH_3)$, phosphine] and proposed that the adduct consists of "electron donor−acceptor complex". The equilibrium constant in the present study is in close agreement with the above values.

At low phosphite concentration, where $k_{obs} = k[P(OMe)_3]$, the reaction is characterized by a large positive volume of activation (+15.7 $cm^3$ $mol^{-1}$) and almost zero entropy of activation and an enthalpy of activation of 90 kJ $mol^{-1}$. In contrast, at high phosphite concentration (rate essentially zero order with respect to $[P(OMe)_3]$), where $k_{obs} = k$, the reaction is described by a small positive volume of activation (+5.5 $cm^3$ $mol^{-1}$), a large negative entropy of activation (−46 J $mol^{-1}$ $K^{-1}$), and an enthalpy of activation of 77 kJ $mol^{-1}$. The apparently disparate activation parameters are in accord with the precursor formation mechanism shown in Scheme 2. The negative entropy of activation for the rate-determining step reflects that there is significantly greater steric congestion in the transition state relative to the ground state which would be expected for a system involving a seven-coordinate presursor complex. By way of comparison, Bassetti and co-workers[32a] reported $\Delta S^{\ddagger} = -84.1$ J $mol^{-1}$ $K^{-1}$ and $\Delta H^{\ddagger} = 78.7$ kJ $mol^{-1}$ for the alkyl migration within the precursor species [($\eta^5$-$C_9H_7$)$Fe(CO)_2(CH_3)$,$PPh_3$] to afford ($\eta^5$-$C_9H_7$)-$Fe(CO)(PPh_3)(COCH_3)$. It is also noteworthy that Bergman and Wax[32b] observed a trend ($k$(2,5-$Me_2$THF) < $k$(2-MeTHF) < $k$(3-MeTHF) < $k$(THF)) in rate constants for the tetrahydrofuran solvent-assisted $CpMo(CO)_3(CH_3)$ migratory insertion reaction which was consistent with steric inhibition of the entering group upon associative activation.

The small positive volume of activation associated with the rate-determining step ($k$) indicates some volume expansion on going from the ground state to the transition state. The value is very typical for a dissociative interchange ($I_d$) ligand substitution mechanism.[64] This presumably arises from steric congestion around the metal atom as a consequence of more W−CO bond lengthening than W−P shortening as the rigid $\eta^3$-[C,N,N′] imine chelate ligand and the $\eta^2$-vinyl group rearranges in the transition state. Furthermore, greater steric congestion would occur in the transition state if the $\eta^2$-vinyl moiety is reluctant to slip into the $\eta^1$ mode. Such a slippage process would also add to an overall volume increase in the transition state. A large negative entropy of activation (−40.2 J $mol^{-1}$ $K^{-1}$) and a small positive volume of activation (+6.2 $cm^3$ $mol^{-1}$) have also been reported for chelate ring closure in (*o*-phenanthroline)$Cr(CO)_5$.[65] This ring closure process involves a highly structured transition state (negative $\Delta S^{\ddagger}$) in which Cr−N bond formation is outweighed by Cr−CO bond breakage in terms of volume changes (small positive $\Delta V^{\ddagger}$). Small positive $\Delta V^{\ddagger}$ values and large negative $\Delta S^{\ddagger}$ values were also reported for the racemization of both $Cr(phen)_3^{3+}$ ($\Delta V^{\ddagger} = +3.3$ $cm^3$ $mol^{-1}$, $\Delta S^{\ddagger} = -56$ J $mol^{-1}$ $K^{-1}$) and $Cr(bipy)_3^{3+}$ ($\Delta V^{\ddagger} = +3.4$ $cm^3$ $mol^{-1}$, $\Delta S^{\ddagger} = -63$ J $mol^{-1}$ $K^{-1}$) which were interpreted in terms of an intramolecular twist rearrangement mechanism without bond rupture.[66]

The large positive volume of activation found at low phosphite concentration (i.e. for $kK$) is a composite value given by $\Delta V^{\ddagger} = \Delta V^{\ddagger}(k) + \Delta V(K)$. The contributions represent the volume of activation for the rate-determining step and the reaction volume for the precursor formation, respectively. Since $\Delta V^{\ddagger}(k) = +5.5$ $cm^3$ $mol^{-1}$, it follows that $\Delta V(K) = 15.7 - 5.5 = +10.2$ $cm^3$ $mol^{-1}$. Thus, precursor formation is accompanied by a volume increase of 10 $cm^3$ $mol^{-1}$! This can only mean that the binding of $P(OMe)_3$ to **3** during this step must involve a major rearrangement of the kinetic $\eta^2$-vinyl complex. This reorganization could partially reflect the actual isomerization process, for instance involving an $\eta^2$ to $\eta^1$ slippage (see Scheme 6). Alternatively, desolvation of $P(OMe)_3$ during the formation of the precursor adduct could also contribute toward the observed overall volume increase. In general, it is difficult to account in an absolute manner for the volume changes associated with the precursor formation. Interestingly, the $\Delta V^{\ddagger}$ value for $kK$ is very close to that determined for the spontaneous isomerization reaction ($k_1$) and emphasizes the overall volume expansion associated with both the spontaneous and phosphite-induced isomerization reactions.

Thus, the observed kinetic behavior and the $P(OMe)_3$-assisted $\eta^2$-vinyl isomerization can be accurately described by a slight modification of the mechanism depicted in Scheme 5. This revised mechanistic rationale is shown in Scheme 7. Instead of an interchange pathway, the second-order dependence describes a process in which a molecular complex is formed in a rapid pre-equilibrium ($K$) with added $P(OMe)_3$ and the kinetic $\eta^2$-vinyl complex **3**. The phosphite activates the system toward rearrangement with concomitant extrusion of CO ($k$) to afford the thermodynamic $\eta^2$-vinyl complex **5** (see Scheme 2). Note that since the CO kinetics were measured at the low end of the saturation curve, it is reasonable to assume that a similar pathway also explains the CO-promoted $\eta^2$-vinyl isomerization.

## Conclusion

We have demonstrated that under mild conditions intramolecular attack by highly fluorinated pendant

(64) (a) van Eldik, R.; Merbach, A. E. *Comments Inorg. Chem.* **1992**, *12*, 341−378. (b) van Eldik, R.; Asano, T.; le Noble, W. J. *Chem. Rev.* **1989**, *89*, 549−688.

(65) Zhang, S.; Zang, V.; Dobson, G. R.; van Eldik, R. *Inorg. Chem.* **1991**, *30*, 355−356.

(66) (a) Lawrence, G. A.; Suvachittanont, S. *Inorg. Chim. Acta* **1979**, *32*, L13−L15. (b) Lawrance, G. A.; Stranks, D. R. *Inorg. Chem.* **1977**, *16*, 929−935.

**Scheme 7**

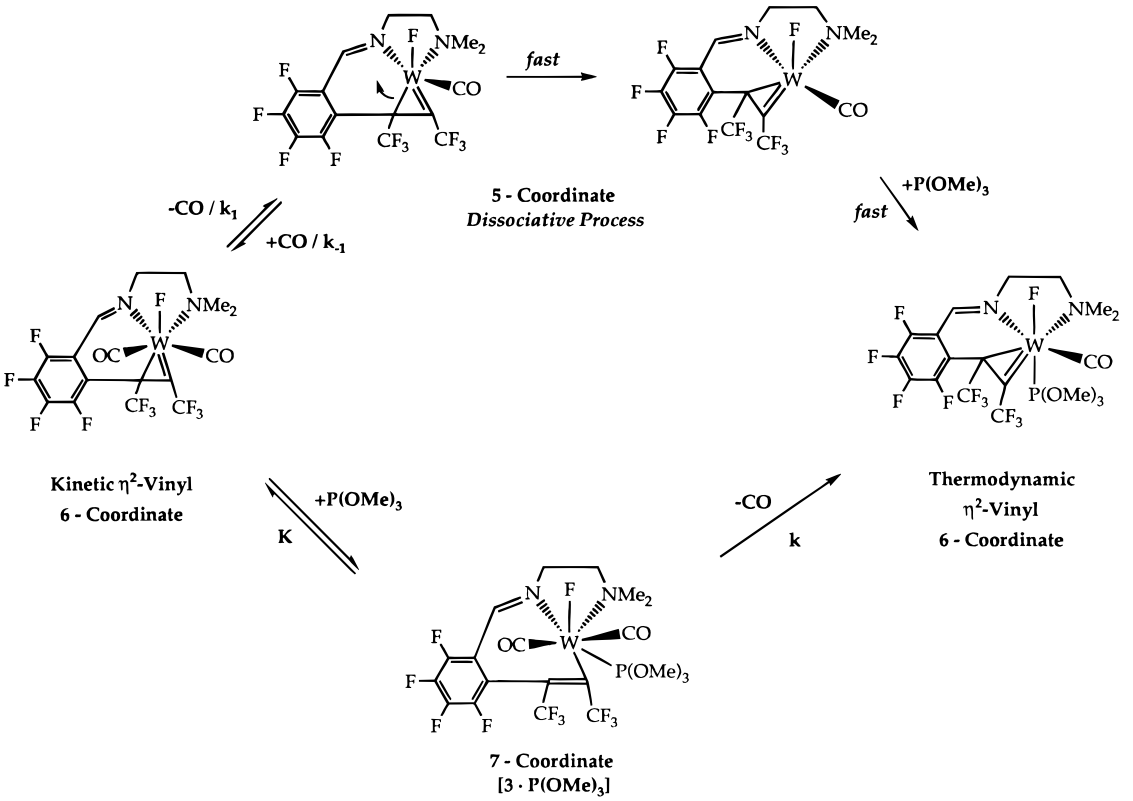


aryl nucleophiles at two-electron donor alkyne ligands affords $\eta^2$-vinyl complexes. Coupled with our carbon−fluorine bond activation chemistry, this allows for net replacement of a carbon−fluorine bond by a carbon−carbon bond. The kinetic $\eta^2$-vinyl complex, *trans*-(L)W(CO)$_2$(F) (**3**), in which the fluoride is *trans* to the inserted acetylene and *cis* to both carbonyl ligands, is accessible through photochemistry. Upon heating, the kinetic $\eta^2$-vinyl complex is converted to a thermodynamic $\eta^2$-vinyl complex, *cis*-(L)W(CO)$_2$(F) (**4**), in which the fluoride is *cis* to the inserted acetylene and *trans* to one CO *cis* to the other carbonyl ligand. In addition to a ligand-independent pathway, kinetic measurements reveal that the isomerization is promoted by added ligand (CO or P(OMe)$_3$). The kinetic measurements and spectroscopic data are in agreement with the rapid and reversible formation of a weak complex between the P(OMe)$_3$ and the kinetic $\eta^2$-vinyl complex, followed by rate-determining rearrangement at the metal center with formation of P(OMe)$_3$−substituted thermodynamic product *cis*-(L)W(CO)(P(OMe)$_3$)(F) (**5**). Importantly, details concerning the intimate nature of the reaction steps were readily obtained from the volumes, energies, and entropies of activation.

Although these ligand-based systems are limited with respect to catalytic chemistry, they clearly serve as model compounds for the systematic studies of structure and reactivity directed toward catalytic activation and functionalization of carbon−fluorine bonds.

**Acknowledgment.** An AAUW American Fellowship to J.L.K. is gratefully acknowledged. The mass spectrometer was purchased with funds from the NSF (Grant CHE-9002690) and the University of Utah Institutional Funds Committee. This research was supported in part by the Alfred P. Sloan Foundation in the form of a Research Fellowship awarded to T.G.R. (1991−1995). R.v.E. gratefully acknowledges financial support from the Deutsche Forschungsgemeinschaft and the Volkswagen-Stiftung. We also thank the Reviewers for useful comments.

**Supporting Information Available:** Tables of observed rate constants as a function of ligand concentration and temperature for all reactions studied, tables giving full crystallographic data for **3**, including bond distances, bond angles, torsion angles, final positional and thermal parameters, and least-squares planes, and a crystal packing diagram for **4** (20 pages). This material is contained in many libraries on microfiche, immediately follows this article in the microfilm version of the journal, can be ordered from the ACS, and can be downloaded from the Internet; see any current masthead page for ordering information and Internet access instructions.

OM9509251